Avdelning för Teknisk Vattenresurslära
ISRN LUTVDG/TVVR-07/5006+72
ISSN-1101-9824

Impact of Coastal Erosion and Sedimentation along the Northern Coast of Sinai Peninsula

Daniel Emanuelsson
Ali Mirchi

Supervisor:
Professor Magnus Larson

Lund Institute of Technology/ Lund University
April 2007

Preface

A study on the impact of coastal erosion and sedimentation on the northern coast of the Sinai Peninsula was conducted as a Masters thesis and the results are presented in this report. The study constituted a part of a larger investigation funded by the Swedish Development Agency SIDA, where research cooperation is undertaken by the Department of Water Resources Engineering, Lund University, Sweden, and Department of Civil Engineering, Suez Canal University, Egypt. The project was carried out in order to provide an understanding of the coastal processes that are predominantly responsible for the erosion and sedimentation problems along the Sinai northern coastline. The thesis work was accomplished under supervision of Professor Magnus Larson at the Department of Water Resources Engineering.

Acknowledgements

We would like to give our genuine gratitude to Professor Hans Hanson for his valuable comments and guidance regarding the modeling of the shoreline change at El Arish. Cooperation with our Egyptian colleagues at the Suez Canal University, especially, Dr. Yasser Hamed, Dr. Ehab Tolba, and professor Mohamed Balah, in providing parts of the source data for the study it is highly appreciated and thanks also for the great hospitality shown during the stay in Egypt, November 2006. The interesting visit to the erosion/accretion sites along the El Arish coastline is also greatly appreciated. We also would like to thank Dr. Badr at the Coastal Research Institute (CoRI) regarding the arrangements made and hospitality shown during the visit to Alexandria.

Finally, our deepest thanks to our supervisor, Professor Magnus Larsson whose valuable guidelines on both technical and administrative matters enabled us to better perform our work throughout this thesis study.

Abstract

Coastal engineering activities during the past five decades have resulted in considerable shoreline change along the northern coast of Sinai Peninsula. In the west of El Arish Power Plant, sediment accretion has reached the tip of the breakwater of the cooling water intake basin necessitating extensive dredging inside the basin. In the east of El Arish Harbor, the shoreline is continuously retreating. Previous activities to mitigate the erosion have not succeeded. For example, the groin field in the east of the El Arish Harbor has transferred the problem to the neighboring beaches farther downcoast.

In this study predominant coastal processes affecting the erosion of the Sinai northern coastline were investigated. Wave-induced longshore currents were found to be responsible for transporting the littoral drift along the coastline. Longshore sediment transport, from Port Said to Ashqelon, was quantified and the general patterns of erosion-accretion were determined by looking upon the gradients between transport rates along the coast. Particular emphasis was placed on shoreline change due to perturbations introduced by infrastructure sited at the coastline near El Arish. The shoreline change at El Arish Power Plant and Harbor were modeled using the coastal evolution model GENESIS. Having understood the coastal processes driving the shoreline change at these two locations, appropriate remedial measures were proposed to mitigate the problem. In this regard, a combination of hard and soft coastal engineering methods are presented to alleviate the dredging problem at the power plant while sand-bypassing/beach-nourishment is suggested as an effective sustainable solution to the erosion problem in the east of El Arish Harbor.

Keywords: Accretion, El Arish Harbor, El Arish Power Plant, Erosion, GENESIS, Longshore Sediment Transport, Shoreline Change Modeling, Sinai Peninsula.

Table of Contents

1. Introduction

1.1 Background

During the last five decades the northern coast of Sinai Peninsula has been intensely exposed to coastal changes that have created many serious problems. These problems can broadly be classified into three major types:

- Erosion of important coastal areas and associated loss of land,
- Sedimentation at lake outlets and harbors,
- Pollution of coastal areas and lakes.

The coastal erosion and sedimentation problems harshly affect both important resort areas and lake fishing grounds threatening the livelihood of Sinai inhabitants. The ongoing present trend may force the inhabitants to eventually leave Sinai and migrate to already crowded areas in the delta and the Nile Valley. Several processes of both natural and anthropogenic origin affect the evolution of the Sinai northern coastal areas. The most important processes may be summarized as follows:

• Development of infrastructure: In the past few decades, development of the Sinai northern coast has called for extensive infrastructural development, for example, El Arish Power Plant and El Arish Harbor. The impact of increasing coastal works to protect the infrastructure, sited at the coastline, on the sediment transport patterns will be discussed later on.

• Impact of local river floods: El Arish Valley and Wadi El Arish practically drain the entire northern and central portion of Sinai. The beach near the outlet of this valley is straight and usually conforms to the behavior of a regular shoreline in balance with the prevailing waves. However, during a short period of time at the end of February 1975, a voluminous flood transported several million cubic meters of water and sediment to the sea. The sediments formed a large new delta with its front located more than 400m seaward of the previous shoreline with a large submarine extension (Hamed, 2007). This new delta partially dammed the longshore sand drift resulting in sediment accumulation on the western flank of the delta, simultaneously as serious downdrift erosion occurred east of the delta. The sediment in the delta was rapidly transported eastwards and the delta changed shape, gradually returning back to an almost straight and regular shoreline. Unfortunately, the beautiful palm beaches of El Arish, east of the delta, have never recovered from the erosion that developed during the formation of the delta.

• Reduction in the natural sediment supply and sand mining/ dredging: Sand dunes are common features in the coastal zone and they constitute an important component in the beach system. Dunes provide protection for low-lying coastal areas in the course of storms. Furthermore, they act as reservoirs of material for the beach and adjacent areas. Previously, large quantities of sand were extracted from the subaerial beach and dunes at an estimated annual rate of 10 to 20 times the naturally occurring annual sand replenishment (by wind, etc.). This extraction caused a sand deficit along many coastal stretches accelerating the erosion of beaches and nearby cliffs/dunes (Hamed, 2007).

Climate

The climate of North Sinai is determined basically by the following factors: The semi permanent pressure in each season, such as the cold Siberian anticyclone in winter, the heat lows of Africa in spring and summer, and the huge low over southwest Asia in summer (Abdel Rahman *et al.*, 2001). Outstanding weather phenomena in the region are the dust and sand storm that blow in the transitional seasons in spring (March to May) and in autumn (September to November). In spring the hot desert depressions, known as Khmasin, are always associated with strong hot dry wind often carrying large quantities of dust and sand (Robaa, 2002). Hence the Khmasin depression is an important factor in the dry sediment transport of material to the coastal zone.

The amount of precipitation over the Sinai Peninsula is limited. Periods with no rain or very small amounts occur from April to October, and the rest of the year rain comes in short, intense downpours. The average annual rainfall for El Arish is about 100mm (Hellström, 1953). The amount of rainfall increases to the north east and decreases to the south west (Abdel Rahman *et al.*, 2001).

1.2 Objectives

Understanding the processes responsible for the coastal erosion along the northern coast of Sinai will provide the authorities and coastal managers with crucial information that will help save important recreation areas and extensive palm tree groves. Additionally, contributions to solve coastal erosion in combination with studies conducted to develop a sustainable society in Sinai, will not only bring prosperity to the people living there but also attract people from crowded areas of Egypt to work and reside in Sinai. Along with the urgent need to alleviate the erosion problem at the Sinai northern coastline, the main objectives of this thesis are to:

- Identify the predominant coastal processes affecting the erosion of the Sinai northern coastline
- Quantify the sediment transport rate along the coastline
- Study the impact of the infrastructures on the shoreline change
- Propose protective measures to alleviate the erosion problem

1.3 Procedure

As a first step towards achieving the objectives of the study, available literature and similar previous research works conducted at the coastline were studied to provide an overall understanding of the problem. The data extracted from the literature together with data obtained from Suez Canal University, were compiled to reveal the extent of data insufficiency. In the next step, a 2-week trip was made to Egypt to visit the study area. The severely accreting-eroding spots along the coastline were visited to improve the physical understanding of the situation. To ensure that the data collected from various sources were usable for modeling, the quality of the data was assessed by performing some preliminary computation to estimate the large-scale longshore sediment transport rate. The data for shoreline position were partly provided through a shoreline measurement program conducted

by Suez Canal University and Coastal Research Institute (CoRI). Finally, the shoreline was modeled using the coastal evolution model GENESIS (Hanson and Kraus 1989) to investigate the shoreline trends and compute the sediment transport rate. Based on the results of the modeling, the site visit, and outcomes of similar projects appropriate protective measures were introduced.

Literature review

Previous research works on coastal processes and, particularly, sediment transport patterns along the northern coast of Sinai were reviewed to help gain an understanding of the general coastal trends within the study area. Besides becoming familiar with the coastline, performing this task was of primary importance in acquiring readily available data. Moreover, the results of some of this work formed a good basis for verifying the data reliability.

Data compilation

Available wave and wind data for the coastline were collected with the help of colleagues in Suez Canal University. The one year measurements of the wind and wave series used in this study were measured at Port Said by Delft Hydraulics from 1999-06-29 to 2000-06-30. Other data requirements, e.g. shoreline position, shoreline orientation, shoreline configuration, fetch length for various segments of the shoreline, sedimentological data, etc. were met using shoreline charts, satellite images, sea charts, and the results of previous investigations.

Site visit

A site visit was made to the El Arish area in November 2006, during which the power plant, the harbor, the new groins (4 km west of the harbor) and the palm beach east of the harbor were visited. The first stop was the Power Plant on the El Masaid coastal zone. According to Frihy *et al.*, (2002) accretion of sand is taking place in the embayment at which the power plant is located. The problem is the considerable siltation of the intake channel for cooling water to the power plant. The channel is continuously dredged every working day of the week. The dredged material from the inlet channel is pumped out to the beach between the water intake and outlet. Additional sand nourishment is done adjacent to the eastern side of the water outlet, to mitigate the local erosion caused by the western breakwater of the intake.

Next the El Arish Harbor was visited. Severe erosion is taking place east of the harbor threatening the palm groves and relict sand dunes. Along the beach an old destroyed groin system consisting of 12 groins is present. Occasionally, with high sea levels or high waves the sand-transporting currents can bypass the landward tip of the groins, causing them to lose much of their original functionality. Figure 1.1 shows the substantial erosion at the beach that exposes the roots of the palms trees. Figure 1.2 shows a closer view of the relict sand dunes. It is possible to distinguish layers of different material composition originating from different geologic time periods. Also, a small landslide caused by undermining of the dune foot can be seen.

Figure 1.1 Exposed roots of palm trees indicating severe erosion along the beach in the east of El Arish Harbor.

Figure 1.2 Erosion of sand dune at the palm beach east of El Arish Harbor.

The last place visited was the newly built groin system. The groin field consists of seven blue-colored groins built 4 km west of the El Arish harbor in 2003, to protect the revetment and resort facilities located close to the beach. At the eastern part of the groin field and east of the groin field there is an area of strong erosion. At parts, the sand has entirely disappeared. Here, the waves are hitting the revetment which now acts as a seawall and partly reflects the waves. The forces from the waves are undermining the revetment and damaging the structure (see figure 1.3). Fine-grained sand is used as replenishment material, but is instantaneously transported away by the longshore current. In the picture it is possible to observe that the sand load is high in the water through the different color nuances of the sea.

Figure 1.3 Undermining of the revetment 4 km east of El Arish Harbor.

Mathematical modeling

Since the erosion-sedimentation problem along the Sinai northern coast is for the most part caused by wave-driven longshore currents (Frihy *et al.,* 2002), results of quantifying the sediment transport rate are deemed highly sensitive to the quality of the wave data. Assuming that the obtained one-year wave data represented a typical year in terms of magnitude of sediment transport rate, a computer program was developed to make a preliminary estimate of the volume of the sediment transported annually. However the wave measurements were found to be partly affected by nearshore conditions. The waves were influenced by the local shoreline orientation at Port Said and therefore failed to represent locations along the Sinai Peninsula that differ to a great extent in shoreline orientation from Port Said. Therefore, available wind data corresponding to the same year were also used as input data to another program to yield the waves generated by winds. Then, in another attempt, the sediment transport program was run by waves obtained from the wind data. As a result, the estimated sediment transport pattern showed a good agreement with the results from previous studies. However, large-scale sediment transport rates calculated from wind and waves turned out to be more similar than first suspected, and the two methods are both able to capture the regional transport pattern along the Sinai Peninsula.

The evolution of the shoreline was described using the GENESIS numerical model (GENEralized Model for SImulating Shoreline Change). Because of GENESIS proven capability in simulating long-term shoreline change produced by spatial and temporal

differences in longshore sediment transport this numerical modeling system was selected to model the Sinai northern shoreline. GENESIS is an efficient model for simulating the response of the shoreline to structures constructed in the nearshore, which is mostly the case at the northern coast of Sinai.

Many unsuccessful attempts have been made to prevent the erosion at the Sinai northern beaches, for example, using a series of groins. As an ultimate product of this study, effective methods to alleviate the destructive coastal erosion, including both appropriate coastal structures and soft solutions (e.g. beach nourishment) are proposed.

2. Coastal Processes at the Sinai Peninsula

2.1 Study Area

The study area lies between longitudes 32°00'E and 34°42'E and latitudes 31°26'N and 31°55'N on the northern coast of Sinai Peninsula. The stretch of interest covers some 325 km of the coastline from west of Port Said extending as far as to the north of Tel Aviv in Israel (figure 2.1). The coastal area at El Arish is the main area of interest for this study. Other areas included are investigated for the purpose of estimating the large-scale sediment transport rates in the region and getting a deeper understanding of the large-scale processes affecting the El Arish coastal area.

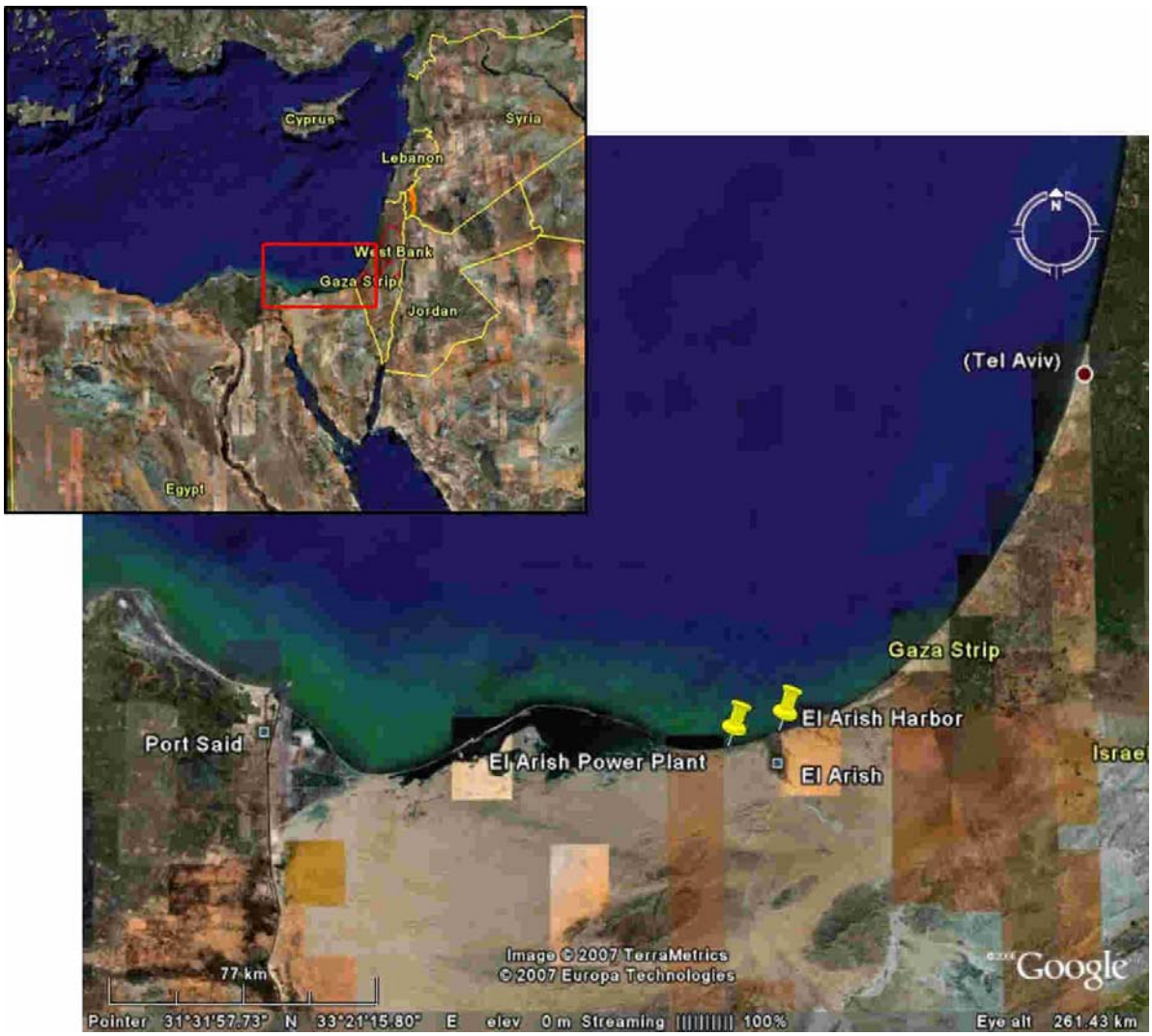

Figure 2.1 Sinai Peninsula northern coastline with the study area from east of Port Said to Tel Aviv, Israel, in the west.

Two protruding headlands at Port Said and the Bardawil bulge coast interrupt the generally smooth coastline. These headlands are separated by two large embayments. The coastline at these embayments comprises sand dunes and lowlands made of saltpans known as sabkha

deposits (Frihy and Lofty, 1997). From Port Said to the west of Bardawil lagoon the coastline is characterized by conspicuous type of landforms namely; sandy shore, coastal plain marginal lagoons, Nile flood plain, sand dune belt and sabkha deposits (Dewidar and Frihy, 2003). To the east of the lagoon the shoreline mainly comprises sandy spit formations, heading to the east, located at the eastern end of the barrier of Bardawil lagoon. The lagoon is separated from the Mediterranean by a 500 m wide and 80 km long, curved, narrow sand barrier. It is connected to the open Mediterranean Sea by three inlets, two artificial and one natural (Frihy and Lofty, 1997).

The coastline is famous for its natural beauty and distinct landforms including a variety of ecosystems and different types of natural areas, such as white sandy beaches, picturesque palm groves, and large brackish lakes.

2.2 General overview

Shoreline trends are governed by various coastal processes such as waves, tides, changing levels of sea, nearshore currents, and longshore transport of sediments on beaches. In this section, some costal processes are introduced in brief that are mainly responsible for the erosion at Sinai northern coastline.

Waves

Wave energy, generated over water bodies, dissipates along the beach through the breaking process. Waves affect morphological characteristics of the coastal zone. They also change the composition of bottom sediments on the shoreface, transport sediments alongshore, offshore and onshore. Furthermore, the great amount of energy brought to the shore by waves is eventually expended in the nearshore zone or on the beach. All this energy dissipating over a short reach creates a powerful force that needs to be considered when designing harbors, shore protection measures, and coastal structures (CEM, Part 4, 2002**).**

Sea level changes

A long-term geological process of importance to a shoreline is relative sea level change, which can occur as the result of a change in water volume of the oceans or the subsidence or emergence of the land by geologic processes (Dean and Dalrymple, 2002). Fenoglio-Marc (2001) investigated the long-term sea level change during 1992-2000 in the Mediterranean Sea using satellite altimetry and tide gage data. In this study the average sea level rise in the eastern Mediterranean Sea was estimated 9.3 mm/year.

Tides

The water level change caused by tidal motion is small along the Sinai Peninsula. The El Arish coastline is classified as a micro-tidal semi-diurnal area and the tidal range is about 30 cm (Frihy *et al.*, 2002).

Storm surge

When surface currents induced by wind from storm events move water towards the coastline it piles up against land, if the storm has sufficient duration and a predominant wind direction towards the coast. The water level will increase and the waves can therefore remove sediment at higher elevation (SPM, 1984). However, major storm events in the El Arish area causing storm surge are not that frequent (see the discussion about wind climate, part 2.3) and therefore is the influence of storm surge assumed to be small and not taken into account.

Nearshore currents

There are two wave-induced current systems in the nearshore zone which dominate the water movements in addition to the to-and-fro motions produced by the waves directly. These are (1) a cell circulation system of rip currents and associated longshore currents, and (2) longshore currents produced by an oblique wave approach to the shoreline (Komar, 1976).

In general, the closer you get to the beach the more dominant the wave-induced currents will be, whereas the influence of the general current patterns (read Mediterranean gyre in our case) will diminish (Larson and Hanson, 1992). Longshore transport of sediments, i.e. wave-driven movement of sand along the coast, is the most dominant coastal process for moving sand in the littoral system of the study area (Frihy *et al.*, 2002). This is manifested by sand accumulation at the structures sited at the shoreline, e.g. western breakwater of the El Arish Power Plant. The longshore sediment transport at the Sinai northern coastline is, for the most part, driven by waves obliquely approaching the shoreline. Frihy *et al.*, (2002) measured longshore currents on both sides of the El Arish Power Plant coastline over a period of about 28 months, from March 1996 through June 1998. This monitoring program showed that the predominant longshore current direction at the noted segment of the coastline is from west to east (62%-65%), induced by waves coming from the NNW and NW. Additionally, westward longshore currents (24%-29%) result from the remaining wave component from the N, NNE and NE sectors.

The Mediterranean gyre is a large scale currents system. The part of the gyre active along the Sinai Peninsula is the Southern Levantine current. The gyre is induced by topographic features, wind and thermohaline forcing. The topographic feature of greatest importance for the Mediterranean gyre is the strait of Gibraltar. The gyre is characterized by a counter clock wise motion due to the Coriolis effect (Pinardi and Masseti, 2000; Millot and Toupier-Letage, 2004).

Longshore sediment transport

The above-noted predominant longshore currents at the northern coast of the peninsula tend to displace and move the sediments parallel to the coastline. The rate of the longshore sediment transport and the direction in which the sediments travel determines in large part the accretion-erosion pattern of the shore. The longshore sediment transport is of primary concern at the Sinai northern coast in that it has resulted in an ongoing build-up of the beach on the updrift side of the infrastructural coastal facilities, for instance, El Arish Power Plant.

Due to the general orientation of the coastline, the longshore sediment transport is almost unidirectionally eastwards all year long, with small westward reversals (Frihy *et al.,* 2002). There are several indicators for eastward longshore sediment transport at the northern coast of Sinai, for example, changes in shoreline position resulting from erosion and accretion trend,

sand accumulation versus beach erosion on opposite sides of jetties, longshore growth of sand spit, and finally, patterns of beach sand variations in grain sizes and mineralogy (Frihy and Lofty, 1997). Moreover, in a three-year long study (1985-1987), Fanos *et al.,* (1994) investigated the coastal processes at the El Bardawil Lagoon and found that the predominant longshore current direction is towards the east causing siltation on the western side of the lagoon's western outlet. This is also confirmed by the results of bottom sediments characteristics where the beach sediment are coarse in the area to the west of the intake (accretion area), fine between the intake and the discharger, and relatively fine to the east where the coastline is eroding (Badr, 2001).

The power plant coastline began to become unstable following the construction of the breakwaters of the water intake basin. The effect of the western breakwater of the power plant intake has diminished while reaching full capacity of deposition on its western side. Consequently, sediments transported by westerly longshore currents started to bypass the breakwater and found their way into the inlet of the intake basin. On the other hand, local reversal in the eastward pattern of sediment transport tends to further intensify the sedimentation problem in the intake basin (Frihy *et al.,* 2002).

Cross-shore sediment transport

Currents associated with nearshore cell circulation act to produce only a local rearrangement of beach sediments. The rip currents of the circulation can be important in cross-shore transport of sand, but there is minimal cross-shore net transport of beach sediments along the coast (CEM, part3, 2002). Offshore shift of sand from the berm to the bars, generally, takes place during storm conditions of large wave activity. During smaller swell wave conditions sand moves in the opposite direction, i.e. sand is transported back onshore and the berm grows (Komar, 1976).

In general, comparatively high waves approach the Sinai northern coastline during the winter (October to March) whereas swell waves are active during the spring and summer (Frihy *et al.*, 2002). This seasonal variation may contribute to onshore-offshore sediment transport at the Sinai Peninsula. However, shoreline change produced by cross-shore sediment transport as associated with cell circulations, storms and seasonal variations in wave climate are assumed to average out over a sufficiently long period of time.

Sand dunes and wind-blown sediments

Coastal sand dunes are different from all other coastal landforms in that they are formed by air rather than water movement. It is the interaction between sand transport by the wind and the vegetative cover that characterizes coastal sand dunes. Air-flow over a sand surface is slowed down by a frictional drag at the surface. The resultant decrease in wind velocity is transmitted up through the flow producing a velocity profile. The effect of the air-flow velocity gradient above the beach surface is to apply a force to the sand grains lying on the surface. This force is represented by wind shear velocity. The wind shear velocity mobilizes the smaller sand grains flicking them into the air, usually vertically upwards. These smaller sand grains finally plunge back into the beach surface exploding a group of grains from the beach up into the air where they too are shot forward to land with an impact that shoots up

even more grains. Soon the whole beach surface downwind of the original grains is in movement. This is the saltation process responsible for dune formation (Pethick, 1984).

Sand dunes back the embayments separating the two protruding headlands at Port Said and the Bardawil bulge along the Sinai northern coast. Here, wind contributes to providing the sea with wind-blown sediments through eroding some of the gently inclined broad coastlines, covered by sand dunes. Additionally, wind releases large amounts of kaolinite and illite-rich dust originating in the African and Middle East deserts over broad areas of the southeastern Mediterranean (Stanley *et al.*, 1998).

2.3 Wind climate

Wind is a key factor in shaping the geomorphology of the coastal zone, both directly and indirectly. The wind indirectly contributes to evolving the coastal geomorphology as the wind stress acts upon a water body generating waves and oceanic circulation (CEM, part 4, 2002).

The wind data used in this project are from Port Said although the main area of concern is El Arish. Below it will be investigated how representative these data are for El Arish. The obtained wind data series is incomplete. The file has two data gaps, the first one between 28 July and 3 August and the second one, which is even larger, between 30 November and 4 January. The Data series consists of 7656 observations and hourly records. Each record consists of three different kinds of wind speeds that are given in the data file, the hourly mean wind speed, the 30s gust wind speed, and 10s gust wind speed. In figure 2.2 and 2.3 the mean hourly wind speed is shown, which is a common way to present wind speed measurements. The direction of the wind is also given, in azimuth angle, for each record. The winds were measured at Port Said Dredging Contractors (PSDC) construction site, a few hundred meters inland (31° 12 42.73 N, 32° 21 31.10 E). The measurements were carried out at a height of 10 m above the ground level (Delft Hydraulics, 1999).

Figure 2.2 provides a histogram of the distribution of wind speed for the one-year wind data (1999-06-29 to 2000-06-30).

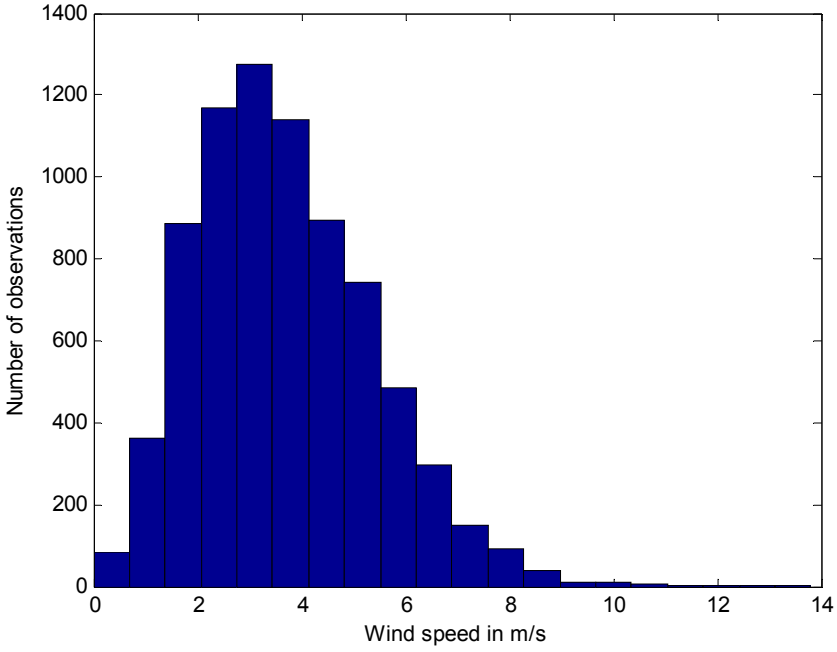

Figure 2.2 Histogram of the wind data with wind speed distribution independent of wind direction.

The wind station at Port Said records wind speed every second. The mean hourly wind speed is the average of recorded values during one hour. The highest peak of the wind speed gust during one hour is identified and the values recorded within a time interval of 10 s or 30 s before the peak occurs are selected to compute the average wind speed for the corresponding gust peak. In this way, an average wind speed is computed for the particular time interval, which gives the 10 s or 30 s maximum wind speed gust (Larsen and Hansen, 2001). The gust speed and the hourly wind speed have a relationship regarding magnitude. In other words, the 10 s gust maximum wind speed is greater than 30 s gust maximum wind speed which is in turn greater than mean hourly wind speed.

The average wind speed for hourly mean records was 3.7m/s. This average wind speed for 1999-2000 can be compared with the average wind speed recorded at El Arish 2.5m/s (Wind Atlas of Egypt, 2005), and with the annual mean of 4.6 m/s for the period 1952-1970 for Port Said (Data extracted from DHI, n.d.).

The most frequently appearing wind directions are WNW to N (see figure 2.3). To be more specific, 35% of the time winds are approaching from these sectors. Statistics for the years 1995-2004 (from the Wind Atlas of Egypt for El Arish, 2005) shows a lower appearance of winds coming from the same sector, 23% (See table 2.1). Figure 2.3 shows the wind rose for the same wind data series. The distribution with regard to wind direction is seen in this figure.

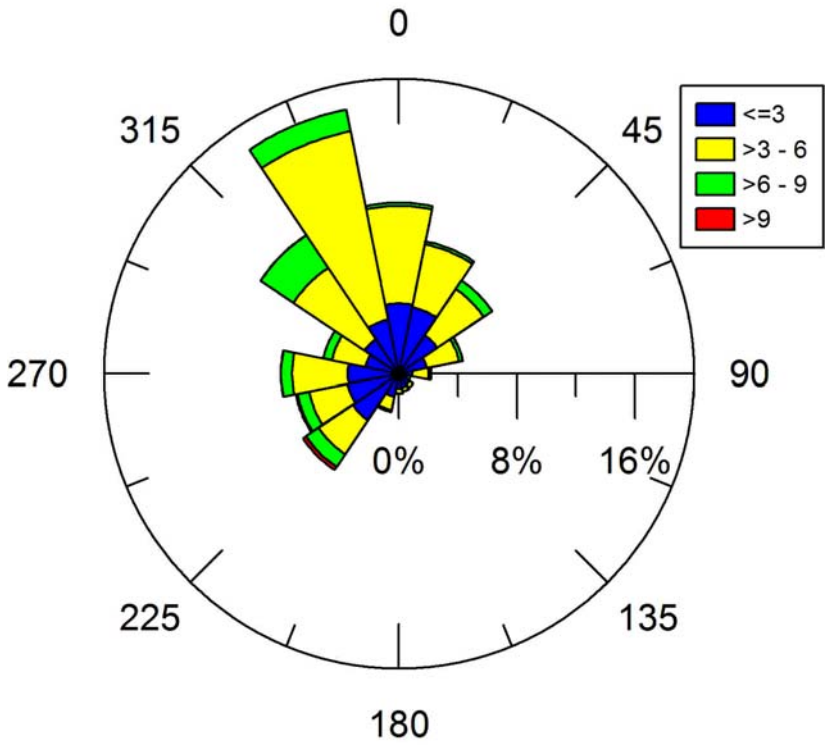

Figure 2.3 Wind rose (m/s) for winds measured at Port Said between 1999-06-29 and 2000-06-30

The strongest winds from the 1999-2000 wind series are, however, coming from SSW to WSW (see figure 2.3). The red color shows the strongest winds. These winds are blowing from land and do not create any waves that approaches the shoreline in the area. But these winds may play a role in the dry sediment transport from the beaches and land to the sea. The strongest wind speed recorded has a velocity of 13.8 m/s and is coming from SW (azimuth angle 218°). This wind speed is not strong enough to be regarded as a storm (wind speed

between 24.5-32.6 m/s), therefore there are no storm events included in this series. Thus, the winds in the series can be regarded as moderate and therefore maybe less representative for the actual wind climate in the region. One support for this statement is that statistics for the wind series from 1952-1970 suggest that 8.1 % of the winds should have a speed of 8.7 m/s (17 knots) or higher. This is not the case in the 1999-2000 series where only 0.59 % has that speed of 8.7 m/s or higher. However, only a small percentage (11.1 %) of the winds of 8.7m/s or higher are approaching from the sea and most of the stronger winds are coming from inland in this series. The data series can also be compared with the wind statistics from El Arish. The wind statistics shows that 33 % of the winds have a speed greater than 8 m/s (Wind Atlas from Egypt). For the data series file the percentage of mean hourly winds with a speed of 8 m/s or greater is only 1.38 %. In the case of 30 s gust maximum wind speed, 8.2 % of the winds have a greater velocity than 8 m/s while11.8 % of the winds with 10 s gust maximum wind speed have a greater velocity than 8 m/s.

There is a daily pattern in the data series from 1999-2000, where the winds are stronger in the afternoon with daily maximum speeds of 6-7 m/s and approaching from NW, and a daily minimum speed of about 2 m/s appear during night (Delft Hydraulics, 1999).

A comparison regarding wind direction frequency between the wind statistics from Port Said from 1952-1970, statistics from El Arish from 1995-2004 and the Port Said wind series from 1999-2000 was performed (see table 2.1) to reveal the representativeness of the wind series of 1999-2000 from Port Said, as an average year, concerning wind direction. The comparison will also show how representative the 1999-2000 series from Port Said are for the El Arish area regarding wind conditions at El Arish. Comparing the 1999-2000 wind rose with 1995-2004 wind rose it is apparent that the frequency of land-to-sea winds are under-represented in the 1999-2000. However, these seaward winds actually fail to generate any breaking waves and, therefore, are not interesting from a sediment transport point of view (see figures 2.3 and 2.4a).

Table 2.1 Frequency of winds blowing in different directions.

	Port Said 1952-1970	Port Said 1999-2000	El Arish 1995-2004
Sect	Freq	Freq	Freq
0	20.5	15.75	14.0
30	10.7	12.0	6.8
60	7.9	7.0	2.3
90	4.8	2.75	2.1
120	2.3	1.25	2.2
150	2.0	1.75	10.5
180	2.5	2.0	12.8
210	4.4	6.0	6.5
240	8.0	10.25	9.0
270	11.0	10.0	8.1
300	8.4	9.5	9.3
330	16.3	22.5	16.5

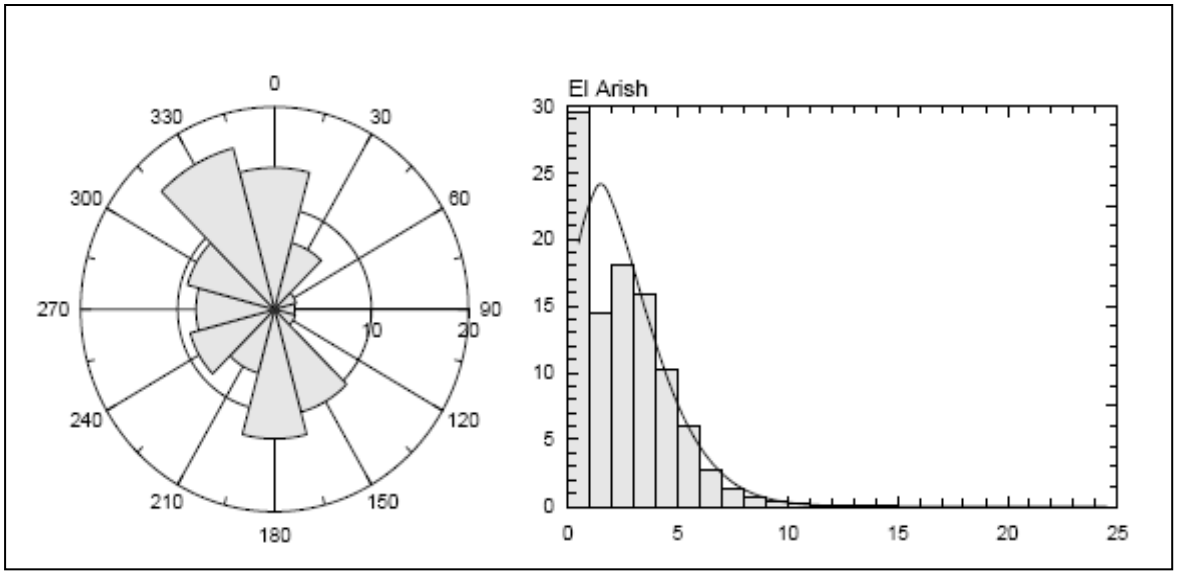

a. El Arish wind rose (1995-2004) b. El Arish wind histogram (1995-2004)

Figure 2.4 a) The wind rose presents the distribution of wind direction at El Arish for the winds recorded between 1995 and 2004. b) The histogram shows the distribution of wind speed (m/s) at El Arish for the winds recorded between 1995 and 2004 (Wind Atlas of Egypt, 2005).

2.4 Sea water level, waves and currents

Sea water level

According to Frihy *et al.,* (2002), the coastline of Sinai is exposed to micro-tidal semi-diurnal tide meaning that the water level varies within a narrow span (< 1 m) and with two high tides and two low tides per day. In this study, the mean high-water level and the mean low-water level at El Arish were found to be 20.22 cm and -11.01 cm, respectively. Therefore the mean tidal range at El Arish shoreline is 31.23 cm (Frihy *et al.*, 2002). Additionally, an investigation preformed at Port Said during spring 1999 showed a tidal range of about 0.4 m (Delft Hydraulics, 1999).

Wave climate

Due to lack of wave records from El Arish, wave measurements from Port Said had to be considered. Wave data from a wave gage located nearshore at Port Said were used in this study. The data series extends over a time period of about one year starting from 1999-06-29 through 2000-06-28. The wave gage took records every third hour including wave direction (DIR), period (T_z), average spectral wave height (H_{m0}), and peak spectral period (T_p). Direction is the main wave direction (coming-from convention) at the highest peak of the spectrum, T_z is computed from m_0 and m_2, the zero- and second-order moments of the spectrum and is a good approximation of the mean wave period T_m, being the average wave period, H_{m0} is computed from the so-called zero-order moment (m_0) of the spectrum and correlates well with the traditional significant wave-height H_s which is the average height (crest-to-trough) of the one-third highest waves, and T_p is the period corresponding to the highest peak of the spectrum (Delft Hydraulics, 1999).

The first 115 records were measured at a water depth of 15 m, between 1999-06-28 and 1999-07-14. Then, there is a 40-day gap in the data set, up to 1999-08-24, owing to interference by a ship. The measurements started again on1999-08-24, but this time the Directional Waverider was installed at 6.3 m water depth. At this depth 2551 records were taken until 2000-06-28. In figure 2.5 the distribution of wave direction and wave heights for direction sectors of 22.5 degrees are presented for this wave series. The predominant direction of wave approach is from sector NNW and N, which comprises 64 % of the record. The average and maximum wave height for the time series are 0.53 m and 2.10 m, respectively.

To be able to compute the sediment transport rate at El Arish, the wave conditions at the coastline need to be known. One way of finding out the wave climate at El Arish was to first bring out the nearshore waves from Port Said to offshore wave condition by considering the refraction pattern with which the waves approached the shoreline (see figure 2.6). Once the offshore wave condition was known the waves were brought back in to other arbitrary locations along the coast including El Arish. In this regard, for simplification, the shoreline was discretized into 6 different segments to derive regional longshore transport patterns based on the azimuth angle of shoreline orientation. Afterwards, using the obtained offshore wave condition, the waves were now propagated towards each shoreline segment. The offshore waves were refracted again as they approached any particular segment at which the wave height at breaking was to be computed. This was achieved using the procedure discussed in chapter 3-1. A computer program was developed for the computations, performing separate calculations for each shoreline segment.

In figure 2.7 the wave climate for El Arish is provided from a study conducted by Frihy *et al.*, (2002). The wave rose is shown to make it possible to judge how representative the wave records from Port Said are for El Arish. According to the study 69% of the waves approach from NNW, NW and WNW.

In figure 2.8, figure 2.9, and figure 2.10 are the wave roses calculated from wind for Port Said, El Arish, and Ashqelon displayed. In part 3.1 are the method for calculating waves from winds further discussed. The measured waves brought offshore (see figure 2.6) and the waves calculated from wind (see figures 2.8, 2.9, and 2.10) have approximately the same predominant wave direction as the waves presented in the wave rose from the Frihy *et al.* (2002) study given in figure 2.7.

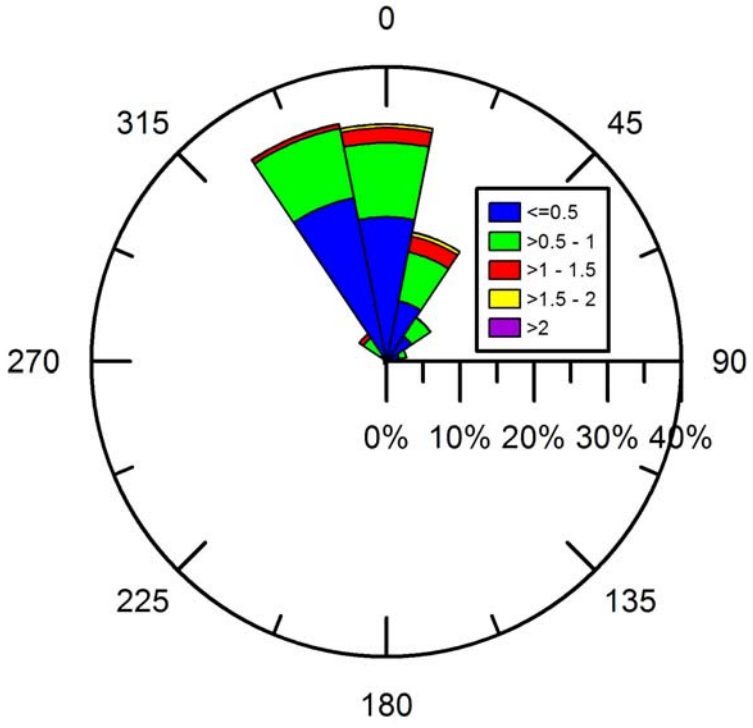

Figure 2.5 Wave rose for waves measured nearshore at Port Said, showing the distribution regarding direction and wave heights [m].

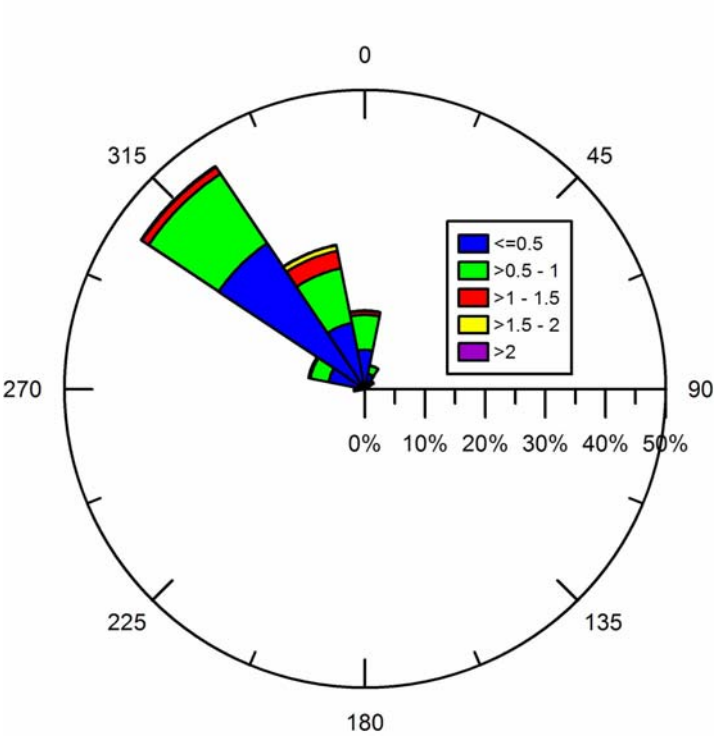

Figure 2.6 Wave rose for Port Said for waves brought offshore, showing the distribution regarding direction and wave heights [m].

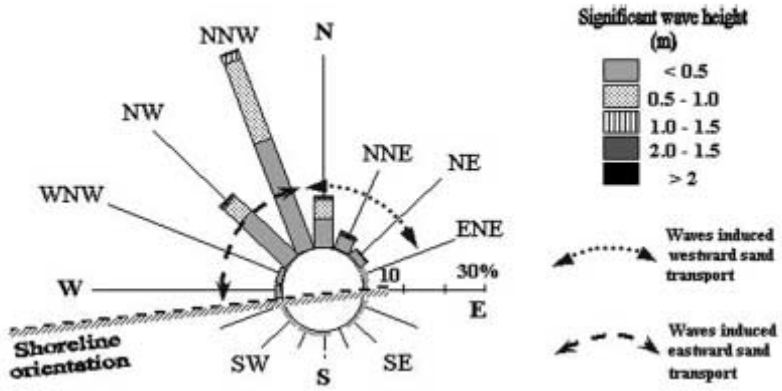

Figure 2.7 Wave rose providing the distribution of wave direction and wave height for El Arish (Frihy *et al.*, 2002).

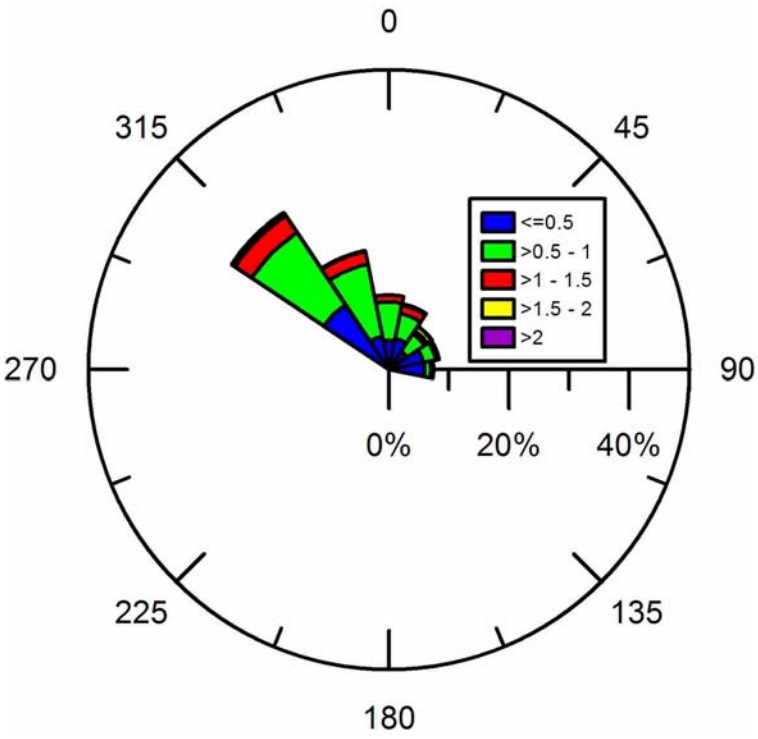

Figure 2.8 Offshore wave rose for Port Said calculated from winds.

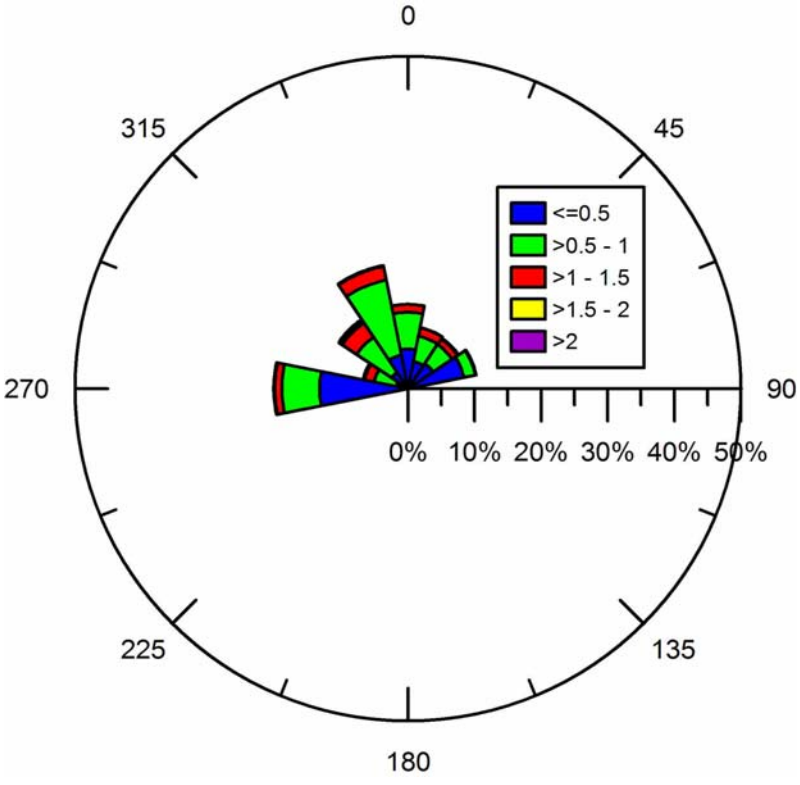

Figure 2.9 Offshore wave rose for El Arish calculated from winds.

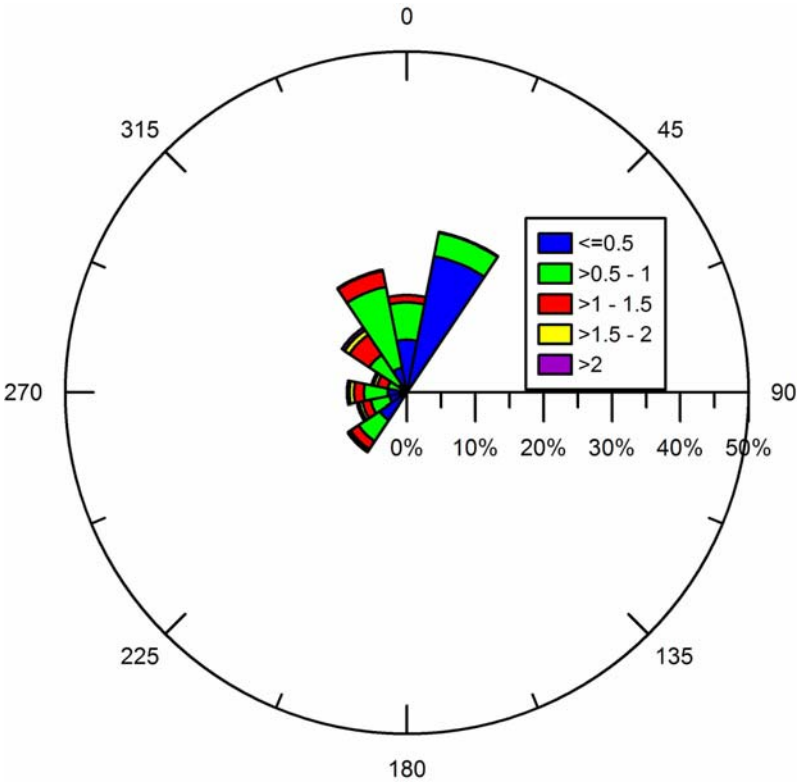

Figure 2.10 Offshore wave rose for Ashqelon calculated from winds.

2.5 Sediment transport patterns

The littoral drift of sediments that occurs along the Sinai northern coast is a part of a larger regional littoral cell, i.e. the Nile littoral cell. The Nile cell, one of the world's longest littoral cells, extends 700 km along the coastline from Alexandria on the Nile Delta to Akziv Submarine Canyon near Akko, Israel (Inman, 2003). Before construction of the High Aswan Dam, the Nile delta shoreline was in a fluctuating equilibrium between sediments supplied by the river and transported away along the coast. Since the construction of the Dam, the main source of sediment to the littoral cell is from erosion of the delta (Inman, 2003). At some parts approximately 15 km of the delta has been taken away by erosion in 100 years (personal conversation with Dr. Bakr, Alexandria 2006).

The sediments eroding from the delta are then transported along the coast. The main force at the delta that causes erosion derives from currents from the Mediterranean gyre. These currents can reach speeds up to 1m/s at shallow delta shelf. The Damietta promontory causes the coastal currents from gyre to separate from the coastline. Sand ribbons constantly form here by the gyre current. The sand ribbons migrate eastward and later further to the southeast towards the coast of Port Said and Bardawil Lagoon (Inman, 2003).

Along the coastline to the east of the Damietta shelf the gyre currents become less important. Here, the main forces driving the eastward currents are induced by breaking waves. The currents form when waves break as they advance towards the beach. As the predominant direction of coming waves is from NNW, NW and WNW, totaling 69 %, the waves most of the time approach the shoreline at angles that trigger an eastward longshore sediment transport (Frihy *et al.*, 2002).

A littoral cell is a coastal compartment that contains a complete cycle of sedimentation including sources, transport paths, and sinks. The boundary between cells is delineated by a distinct change in the longshore transport rate of sediment. In places, waves and currents change locally in response to complex shelf and nearshore bathymetry, giving rise to subcells within littoral cells (Inman, 2003).

The regional Nile Cell can be divided into smaller subcells, each one of these cells has a local stretch where material is taken from the beach, e.g. a source area or erosion area, and a stretch where sediments are accumulating in an area of accretion. These patterns of local erosion and accretion along the shoreline are due to local changes in the net transport rate.

At eroding segments of the coastline the net transport is increasing and the largest net transport occurs out of the compartment, so as long as this condition prevails beach material is constantly eroding. The beach acts as an unwanted local source for the sediment load transported by the currents.

When there is a decrease in the net transport rate between incoming and outgoing transport in a compartment, sediment accumulation takes place on the beach resulting in accretion. The magnitude of accretion will equal the difference between volumes of the transported sediments to-and-fro the compartment. This is where beach acts as an accumulation spot for the transported sediment load.

The Bardawil subcell, among others, is of utmost importance within the study area. This subcell includes the shorelines of special concern in this study at El Arish, and shows the general transport pattern along this stretch. In the Bardawil subcell sand is eroding from the Bardawil bulge barrier and sediments are transported downcoast in an east and south east direction causing accretion at the El Arish embayment and the power plant coastline (Frihy *et al.*, 2002).

According to a study performed by Inman (2003), the longshore sand transport from the Bardawil Lagoon is about 500 000 m^3/yr and gradually decreases to the north with the northerly bend in coastline. This divergence in the littoral drift of sand results in the build-up of extensive dune fields along the coasts of the delta, Sinai, and Israel. The estimation was based on aerial photos of trapped sand on the western side of the Bardawil lagoon inlet jetties (Inman, 2003).

2.6 Human influence on the coast

The increasing recreational and industrial activities on the Sinai northern coast have required extensive infrastructural development including construction of holiday resorts, harbors, power plant, and shore protection works. This rapid infrastructural development is believed to be one of the main causes of the serious coastal erosion. For example, development along the northern coast of Sinai has included the jetties protecting the inlets of Bardawil lagoon as well as the water intake and outlet at El Arish Power Plant, the El Arish Harbor, and the protective groins east of El Arish Harbor. One example of infrastructure projects that have intensified the coastal erosion at the Sinai northern coast are El Arish Harbor. Sand mining from the beach as a source of construction material for development activities has produced a sand deficit along many coastal stretches causing accelerated erosion of beaches and nearby cliffs/dunes (Rosen, 2002). Consequently, the absence of Nile

sediment input coupled with additional sediment loss due to sand mining makes it possible for the waves and currents to actively erode the protruded coast of Sinai.

In addition to the mentioned cut-off in the volume of sediment supply to the Sinai northern coast, man-made coastal structures, e.g. El Arish Power Plant and El Arish Harbor, obstruct the net longshore sand transport. The shoreline has advanced west of the El Arish Power Plant and El Arish Harbor. Simultaneously, corresponding erosion has occurred in the immediate eastern vicinity of these structures. This exacerbates the situation at the sediment-deprived beaches on the downdrift side of the structures.

The severe erosion at the structures sited on the shoreline tends to destabilize them. In several cases, poorly constructed structures have failed under harsh destabilizing effects of erosion and lost their functionality. Furthermore, sand mining for construction purposes can be identified as an anthropogenic factor causing local sediment deficit along the beach. However, it is not possible to quantify the sediment loss due to this factor as there are no sand mining records available.

3. Nearshore Hydrodynamics

3.1 Calculation of wave conditions

Computing wave climate from wind data

It is suspected that the nearshore wave climate at Port Said, where wave measurements were conducted, is not representative for the majority of other locations since the orientation of the shoreline varies greatly along the coast east of Port Said. Additionally, due to presence of the Damietta promontory to the west of Port Said the wave gage fails to record the waves that would otherwise reach the shoreline if the headland were not there. Therefore, it is inferred that the incomplete wave data recorded at Port Said could be used site specifically, i.e. at Port Said only. For these reasons, it was decided to generate waves from the available wind data. By so doing, a general wave climate was obtained that included all approaching waves and was representative for the entire studied coastal stretch. The correctness of the calculations was examined by comparing the waves generated from wind data with available measured waves from Port Said. Detailed discussion on the sediment transport rate computed using each of the noted data sets is presented in Chapter 4.

The wave climate is mainly dependent on the wind conditions, the size of water body over which the wind is active, the water depth, and the mechanism by which the wind energy is transferred to the water surface (Larson and Hanson, 1992).

The winds are driven by large-scale pressure gradients in the atmosphere and tend to even out these gradients. The pressure gradients are assumed to be in a steady state in the following computations. The wind above the wave field can then be considered as a profile. Below 1000 m, the wind conditions will be affected by frictional effects from the sea. Also, the wind speed and direction in this profile will depend on the elevation above mean sea level, surface roughness, temperature difference between air and sea, and temperature difference in the horizontal plane (SPM, 1984).

However in the computation of wave climate from wind condition performed within the framework of this project all of these factors were not considered for simplification. The computation was based on the procedure and recommendations proposed in the SPM (1984). For instance, temperature difference in the horizontal plane is not included in the SPM simplified calculation procedure. Below follows a description of the method applied including equations and assumptions used in the computation process.

The wind series from Port Said were used in the calculation. Here, the used values of wind speed and direction were assumed to be constant during one hour until the next record was made. The calculations were preformed with the different types of wind speeds recorded i.e. mean hourly, 30s gust and 10s gust wind speed, to see which wind-generated waves for Port Said that gave the best correspondence with the measured waves at Port Said.

The wind speed needs to be corrected, in a special order, with respect to a variety of factors. First, the correction for elevation difference has to be taken into consideration. The wind data are measured at an elevation of 10 m above the ground level. The difference between ground and sea level is considered negligible as the wind gage is located only some hundred meters away inland from the shoreline and the coastal area displays a flat topography.

Local effects can disrupt the measurements at the wind station. Given the proximity of the wind station to the sea and absence of tall buildings in its vicinity, the disruptive local effects were also neglected in the computations. In the next step, the wind should be corrected for air-sea temperature differences. However, this could not be done owing to lack of the necessary data. Therefore the temperature differences were assumed to be zero meaning that the boundary layer has neutral stability.

The wave growth formulas are expressed in terms of the wind stress factor U_A or as it is some times called adjusted windspeed. The wind stress factor account for the nonlinear relationship between wind stress and wind speed U in m/s and is expressed as:

$$U_A = 0.71U^{1.23} \tag{3-1}$$

The adjusted wind speed can be used for predictions of the spectral wave height H_{m0} and peak spectral period T_m of the waves in deep water. Two different conditions can prevail: The waves can be either fetch-limited or duration-limited. In the case of fetch-limited wave conditions, the waves are limited by the length of the waterbody over which the wind blows. The wind has blown at a constant speed long enough for the conditions at the end of the fetch to reach equilibrium.

Deep water conditions prevail when the relative water depth $\left(h/L\right)$ is greater than ½, and under these conditions the wave characteristics are independent of depth (SPM, 1984):

$$H_{m0} = 5.112 \cdot 10^{-4} U_A F^{1/2} \tag{3-2}$$

$$T_m = 6.238 \cdot 10^{-2} \left(U_A F\right)^{1/3} \tag{3-3}$$

$$t_m = 32.15 \left(\frac{F}{U_A}\right)^{1/3} \tag{3-4}$$

where h is the water depth, L is the wavelength, F is the fetch length and t_m is the fetch duration, which is given by the time it takes for the wave to travel the whole fetch length.
The calculated wave height and period also need to be checked so that they do not exceed the values for fully developed sea. The equations giving the wave height, period and the duration t_f needed for fully developed sea conditions are:

$$H_{m0} = 2.482 \cdot 10^{-2} U_A^{\,2} \tag{3-5}$$

$$T_m = 0.83 U_A \tag{3-6}$$

$$t_f = 7.296 \cdot 10^3 U_A \tag{3-7}$$

If the duration of the wind t_v is shorter than the time it takes for the wind to travel the fetch length t_m, then the waves are duration-limited. Under duration-limited conditions the wave heights are limited by the time the wind has blown. As stated earlier, it is assumed that the winds blow at a constant speed over the one-hour time interval, (t_v) between two consecutive records.

If the waves are duration-limited ($t_v<t_m$) the duration t_v are substituted into equation 3.4 instead of t_m and an equivalent "fetch length" is calculated. This imaginary fetch length can then be used to calculate H_{mo} and T_m from equation 3.2 and 3.3, for duration-limited conditions.

The wavelength for deep water conditions is given by:

$$L_o = \frac{gT^2}{2\pi} = 1.56T^2 \tag{3-8}$$

where T is the period of the waves and g the acceleration due to gravity. The deep water celerity C_0 and deep water group speed $C_{g,0}$ is given by equation 3.9 and 3.10, respectively (SPM, 1984).

$$C_o = \frac{L_o}{T} \tag{3-9}$$

$$C_{g,o} = \frac{1}{2}C_o \tag{3-10}$$

Wave predictions from wind can be done empirically for shallow water conditions. The wave growth factors are the same as for deep water conditions. The difference here is that for shallow water conditions factors such as bottom friction and percolation in the permeable sea bottom, which reduce the wave height are taken into consideration. The wave height will be smaller and the period will be shorter for waves in transitional or shallow water. The following equations are given for waves generated in shallow water, where equation 3.17 is used in the same way as equation 3.4, to find out if the waves are fetch-limited or duration limited:

$$\frac{g\,H_{m0}}{U_A^{\,2}} = 0.283\tanh\left(K_1\right)\tanh\left(\frac{K_2}{\tanh\left(K_1\right)}\right) \tag{3-11}$$

$$\frac{g\,T_m}{U_A} = 7.54\tanh\left(K_3\right)\tanh\left(\frac{K_4}{\tanh\left(K_3\right)}\right) \tag{3-12}$$

$$K_1 = 0.53\left(\frac{gh}{U_A^2}\right)^{3/4} \tag{3-13}$$

$$K_2 = 0.565\left(\frac{gF}{U_A^2}\right)^{1/2} \tag{3-14}$$

$$K_3 = 0.833\left(\frac{gh}{U_A^2}\right)^{3/8} \tag{3-15}$$

$$K_4 = 0.0379\left(\frac{gF}{U_A^2}\right)^{1/3} \tag{3-16}$$

$$\frac{gt_m}{U_A} = 537\left(\frac{g\,T_m}{U_A}\right)^{7/3} \tag{3-17}$$

A method that takes into account the wave evolution at the previous time step was employed to improve the wave predictions (Dahlerus and Egermayer, 2005):

$$\frac{dH}{dt} = \varphi\left(H_{eq} - H_{in}\right) \qquad (3\text{-}18)$$

where dH is the wave height change that occurs during one time step dt (taken equal to t_m), φ is a constant, H_{eq} is the new equilibrium height, and H_{in} is the wave height from the previous time step. By equation 3.18 the wave will be able to grow or decay from the wave height of the previous time step:

$$H = H_{eq} - \left(H_{eq} - H_{in}\right)e^{-\mu\frac{t}{t_{\lim}}} \qquad (3\text{-}19)$$

where t_{lim} is the limiting duration (taken equal to t_m), t is the duration, of the wind measurement and μ is a constant, which is determined by a least-square fit method to the SPMs wave growth function. If the wind changes and start to approach from a direction which can not generate any waves the waves will decay towards zero and have the same direction as the last waves that could be generated by the wind. The same type of relationship shown for the wave height in equation 3.18 and 3.19 are also assumed to be valid for the wave period.

3.2 Offshore wave conditions

The fetch lengths and depths used in the calculations are presented in table 3.1 and 3.2. The fetch lengths were measured using a sea chart covering the east part of the Mediterranean Sea (Gulf of Sollum to Iskenderun Korfezi, 56031) and the geographic software Encarta were used to obtain a few fetch lengths that were too long to be measured on the sea chart. Three locations were strategically chosen to get a representative pattern of the wave climate at the Sinai Peninsula that is, Port Said, El Arish, and Ashqelon. Fetch lengths and corresponding depths are given in table 3.1 and table 3.2, respectively.

Table 3.1 Fetch lengths for different directions given in km for Port Said, El Arish, and Ashqelon.

	Port Said	El Arish	Ashqelon
1.N	407	411	441
2.NNO	644	496	81
3.NO	407	122	0
4.ONO	244	61	0
5.O	174	30,5	0
6.OSO	0	0	0
7.SO	0	0	0
8.SSO	0	0	0
9.S	0	0	0
10.SSV	0	0	0
11.SV	0	0	70
12.VSV	0	0	130
13.V	0	133	778
14.VNV	0	1840	952

15.NV	695	763	815
16.NNV	593	685	359

Table 3.2 Depths used along fetch lengths given for different directions.

	Mean Depth		
	Port Said	El Arish	Ashqelon
1.N	500	500	500
2.NNO	500	500	40
3.NO	500	55	0
4.ONO	500	25	0
5.O	20	10	0
6.OSO	0	0	0
7.SO	0	0	0
8.SSO	0	0	0
9.S	0	0	0
10.SSV	0	0	0
11.SV	0	0	30
12.VSV	0	0	50
13.V	0	10	500
14.VNV	0	500	500
15.NV	500	500	500
16.NNV	500	500	500

The Fetch lengths, depths and wind data were provided as input data to the computer program that encompassed the equations (3.1)-(3.19) described above. First the conditions at Port Said were considered, because at Port Said it was possible to compare the computed wave height with the wave height records measured by the wave gauge. Wave height series were generated for the three different wind speeds (mean wind speed, 30 s gust wind speed, and 10 s gust wind speed), and these series are plotted together with the measured record of wave heights, in figure 3.1. The figure makes it possible to determine the wind-generated wave height series that yields the best fit with the measured record. The 30 s gust wind speed gave the best fit between the series, as seen in figure 3.1b.

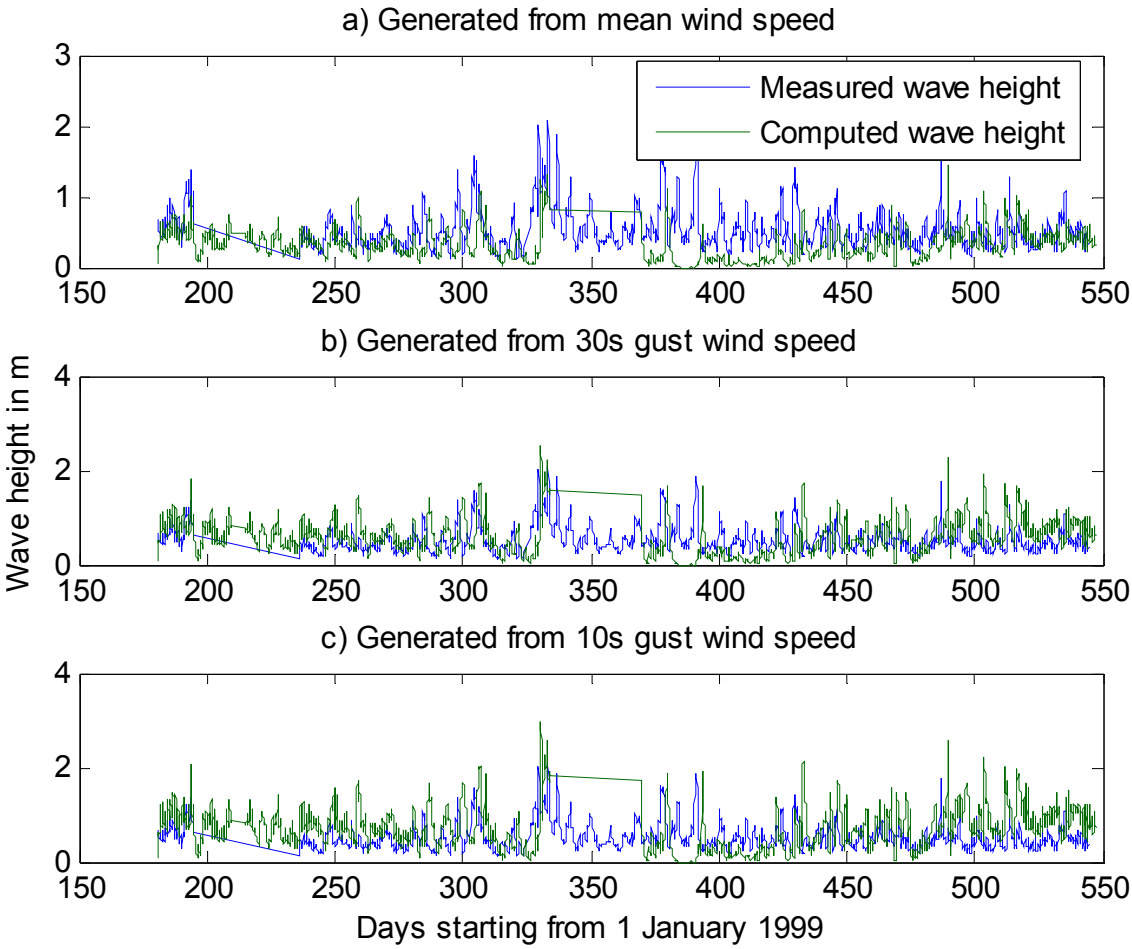

Figure 3.1 Comparison between measured wave height series for Port Said and those calculated from **a)** mean wind speed **b)** 30 s gust wind speed **c)** 10 s gust wind speed.

By running the computer program, using 30s gust wind speed, the offshore wave conditions were generated for Port Said, El Arish and Ashqelon. The frequency distributions of the wave height at these locations are provided in figure 3.2. The wave heights were calculated at a water depth of 20m.

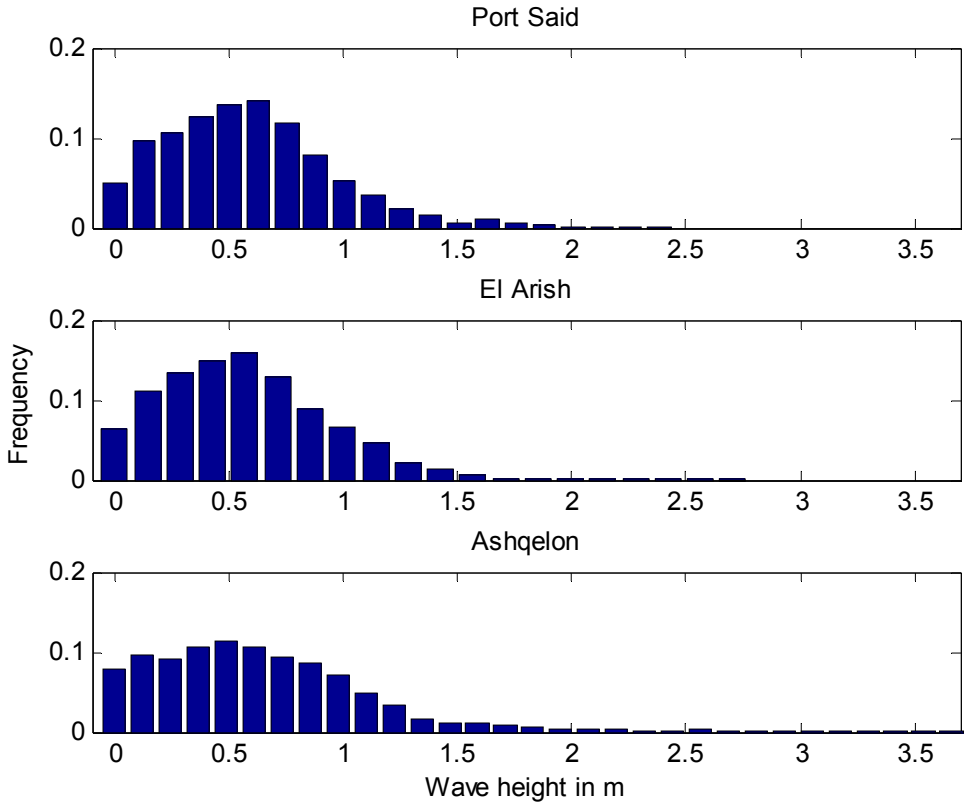

Figure 3.2: Frequency distribution of offshore wave heights for Port Said, El Arish, and Asqelon.

The average wave height, maximum wave height, and frequency of occurrence of wave heights equal to or greater than 1m is provided in table 3.3 for Port Said, El Arish, and Ashqelon.

Table 3.3: Shows information about the calculated waves in terms of maximum wave height, average wave height, and frequency of occurrence of wave heights equal to or greater than 1m.

	Hmax (m)	Haverage (m)	H≥1 (%)
Port Said	2.51	0.59	12.0
El Arish	2.85	0.57	12.3
Ashqelon	3.66	0.63	17.5

To be able to reproduce the shoreline change in GENESIS, it was important to have a complete wave data file for an entire year. To generate a complete wave file from available wind data, the two gaps in the wind data file were filled using the data from the closest time interval with the same lengths from the same wind series. In this regard, the gaps between July28-August3, 1999, and November29-Janury4, 2000, were filled with corresponding values from the side of the gap which showed a better agreement with wind statistics from the wind atlas of Egypt for El Arish. A complete wind data file which covers one year was built in this way. This wind data file was input to a computer program to generate the input wave data file for GENESIS. Inter-annual variation of the wave climate could not be accounted for in the simulations as we only had one year of data. Fortunately, the available wind data captured the representative year regarding the direction of the wind.

3.3 Nearshore wave conditions

When the waves approach the shore and reaches shallow water, where the relative water depth (h/L) is less than ½, bathymetry begins to influence the characteristics of the waves. Refraction, diffraction, shoaling, and reflection are factors that will influence the wave characteristics. It is important to have knowledge about the conditions at breaking (nearshore conditions) to be able to (Larson and Hanson, 1992):

- Estimate the magnitude and direction of wave-induced nearshore currents.
- Estimate the sediment transport rate caused by the wave-induced currents.
- Design coastal structures, taking the force from breaking waves into consideration.
- Account for the setup caused by waves approaching and breaking with a predominant direction towards the shoreline that can result in increased water level.

If the wave crest moves towards the shore at an oblique angle to the bottom contours, the part of the wave which is moving in deeper water will have a higher celerity than the part of the wave traveling in shallower water. This phenomenon causes the wave crest to become more parallel to the bottom contours (refraction) (SPM, 1984).

In this sub-task of the project the bottom contours are assumed to be straight lines parallel to the general shoreline orientation, which is a simplification. In reality the bottom topography is more complex. However, this assumption gives good estimates if the actual contour lines, are not too curved. In order to get a representative one-dimensional model of the bottom contours along the northern Sinai Peninsula coast, based on the orientation, the shoreline was compartmentalized into six different segments in which offshore contours could be assumed parallel to the shoreline (see figure 3.3 and table 3.4).

Table 3.4 Six different shoreline compartments based on the azimuth angle of shore normal for each individual shoreline orientation along the northern Sinai Peninsula.

Wave Climate	Shoreline Orientation
Port Said	34°
Port Said	345°
El Arish	18°
El Arish	347°
Ashqelon	321°
Ashqelon	303°

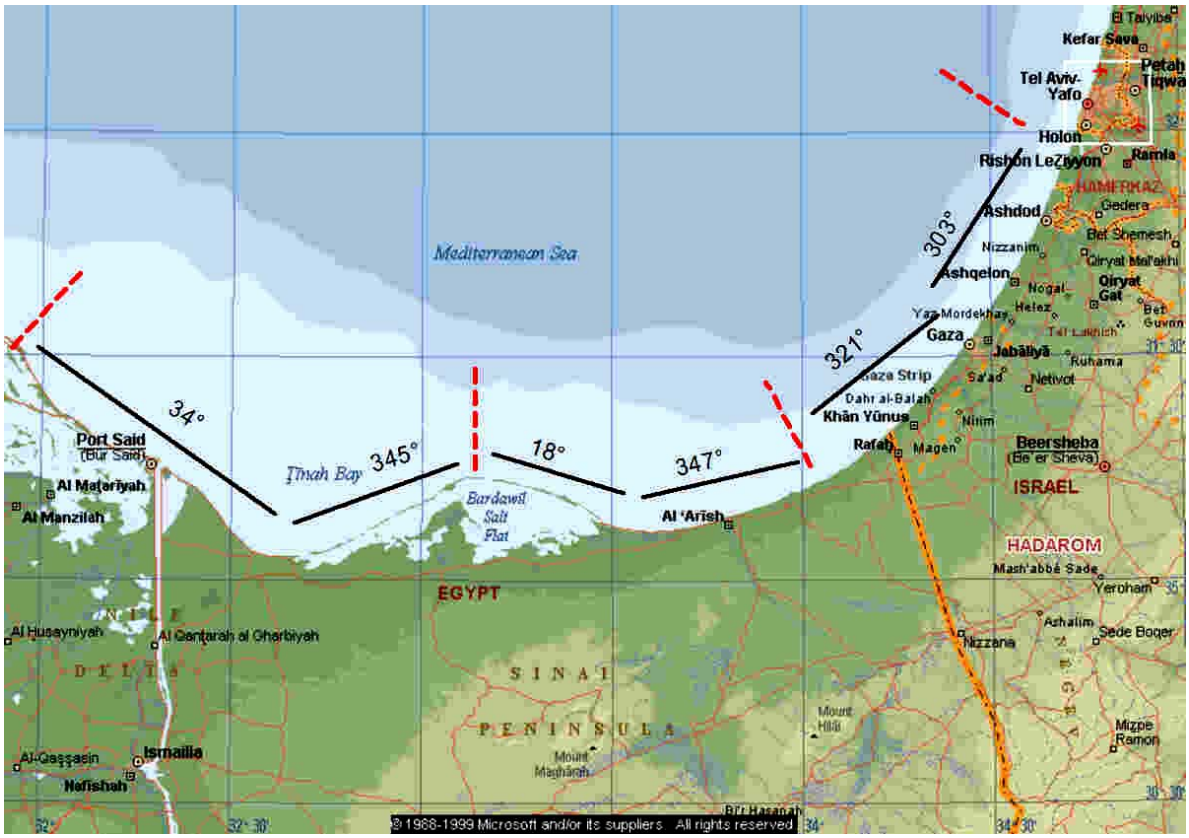

Figure 3.3 The red dashed line shows the boundaries between different compartments of wave climate for the Ports Said, El Arish, and Ashqelon area. The numbers on the black lines present the azimuth angle of shore normal for each individual shoreline orientation along the coast.

In chapter 4 the nearshore sediment transport rate at different segments of the coast will be calculated. For this purpose it is convenient to use a local, right-handed coordinate system. In this coordinate system waves approaching normal to the shoreline are given an angle of 0°. Waves approaching from the right have negative angles and waves approaching from the left have positive angles. The relationship between azimuth and right-handed coordinate systems is given by the expression.

$$\alpha_o = \theta_N - \theta_o \qquad (3\text{-}20)$$

where α_o is the offshore wave angle relative to the shoreline, θ_N is the azimuth angle of the outward normal to the shoreline, and θ_o is the azimuth angle with which the waves are approaching.

Waves with larger α_o angles than $\pm 90^\circ$ will be excluded (CEM, 2002, part 3). Waves with these angles are not represented because of the nearshore conditions prevailing, where land makes a great impact on the wave characteristics. These small waves (considered small because they have hade short time and fetch to grow on) will anyhow move from shore towards the sea and hence not contribute to sediment transport in the area.

Breaking waves

To determine under which conditions the waves are breaking and the characteristics of these waves, linear wave theory was applied. The waves start to break when a certain ratio is reached between the wave height and the water depth known as the breaker depth index, γ_b (the index b is used to indicate conditions at breaking):

$$\gamma_b = \frac{H_b}{h_b} = 0.78 \qquad (3\text{-}21)$$

where H_b is the wave height at breaking and h_b is depth at breaking.

A value often used for the breaker depth index is 0.78, however in reality the index is not constant, it is dependent on factors such as the slope of the beach and steepness of the waves. For beaches with steep slopes the breaker index can increase to values larger than 1.0 (SPM, 1984; CEM, 2002, part 3).

It is important to have a good knowledge about the breaking wave conditions in the area, since wave breaking is an important factor in many nearshore processes. The energy the waves are dissipating can affect coastal structures and therefore has to be considered in the design. If the waves break with an oblique angle to the shore, nearshore currents will be generated. Turbulence caused by the breaking waves mobilizes sediments which then can be transported by the nearshore current. Wave breaking also causes wave setup (Larson and Hanson, 1992).

The equations below are derived from linear wave theory, and are used to derive an expression from which the breaker depth h_b can be calculated. Once h_b is known the wave height at breaking H_b is obtained using the breaker depth index relationship stated in equation 3.21.

The expression for energy flux per unit width F is given by:

$$F = EC_g \cos\alpha \qquad (3\text{-}22)$$

where E is the energy density, C_g is the group velocity for the approaching waves, and α is the angle between the incoming wave crests and the shoreline orientation/bottom contours. The energy density per unit area is given by:

$$E = \frac{1}{8}\rho g H^2 \qquad (3\text{-}23)$$

where ρ is the density of water.

Snell's law can be applied in cases of straight shorelines with parallel bottom contours. By applying Snell's law the effect of refractions is accounted for (SPM, 1984). The index o is used to indicate offshore conditions:

$$\frac{\sin\alpha_o}{C_o} = \frac{\sin\alpha_b}{C_b} \tag{3-24}$$

where C_o is offshore wave celerity, C_b is the celerity at breaking, α_o is the angle between the offshore wave crests and the shoreline, and α_b is the angle between the breaking wave crests and the shoreline. The calculations with Snell's law can be carried out between different locations in the nearshore zone, and here refraction between the offshore and break point is considered.

The general expression for the group celerity $C_{g,i}$ is obtained as follows:

$$C_{g,i} = nC_i \qquad i = o,b \tag{3-25}$$

$$n = \frac{1}{2}\left(1 + \frac{4\pi h_i / L_i}{\sinh\left(4\pi h_i / L_i\right)}\right)$$

The wave celerity and the group celerity for waves in deep water condition is given by, respectively:

$$C_o = \sqrt{\frac{gL_o}{2\pi}} \tag{3-26}$$

$$C_{g,o} = \frac{1}{2}C_o \tag{3-27}$$

The celerity and group celerity for breaking waves are approximately equal for shallow water conditions:

$$C_b = C_{g,b} = \sqrt{gh_b} \tag{3-28}$$

To obtain the wave length L_b and group speed $C_{g,b}$ at breaking the dispersion equation is solved, by applying a subroutine in the Fortran code.

By merging equations 3.22 and 3.23, one expression is obtained for calculating the energy flux:

$$F = \frac{1}{8}\rho g H^2 C_g \cos\alpha \tag{3-29}$$

Assuming that the energy loss due to bottom friction for waves approaching the beach is negligible until incipient breaking condition is reached the offshore energy flux can be set equal to the energy flux at breaking, to yield the following expression based on the energy flux conservation:

$$H_o^2 C_{g,o} \cos\alpha_o = H_b^2 C_{g,b} \cos\alpha_b \tag{3-30}$$

By using equation 3.30, Snell's law (3.24), and the different expressions presented for the wave at deep and shallow conditions, it's possible derive a single expression where the only unknown variable is the depth at breaking h_b (Larson, Kraus and Hanson, 2002):

$$\left(\frac{h_b}{L_o}\right)^{5/2} \cos\left(\arcsin\left(\sqrt{2\pi}\sin\alpha_o\sqrt{\frac{h_b}{L_o}}\right)\right) = \left(\frac{H_o}{L_o}\right)^2 \frac{\cos\alpha_o}{\gamma_b^2 2\sqrt{2\pi}} \qquad (3\text{-}31)$$

For small angles of breaking ($\cos\theta_b \cong 1.0$) equation 3.31 can be simplified into:

$$\frac{h_b}{L_o} = \left(\left(\frac{H_o}{L_o}\right)^2 \frac{\cos\alpha_o}{\gamma_b^2 2\sqrt{2\pi}}\right)^{2/5} \qquad (3\text{-}32)$$

The breaking angle (α_b) for the incoming waves is given by:

$$\alpha_b = \arcsin\left(\sqrt{2\pi}\sin\alpha_o\sqrt{\frac{h_b}{L_o}}\right) \qquad (3\text{-}33)$$

A computer program was implemented to make the calculations for offshore waves approaching the shoreline from 20m water depth to the break point. Because of the shoreline orientation some offshore waves will not be taken into consideration, as they will be shadowed by land at nearshore conditions. The frequency distribution of breaking wave height for Port Said, El Arish, and Ashqelon is given in figure 3.4. Table 3.5 provides statistics for the breaking waves at the different locations in terms of the maximum breaking height, mean breaking height, and frequency of occurrence of breaking wave height greater than or equal to 1m.

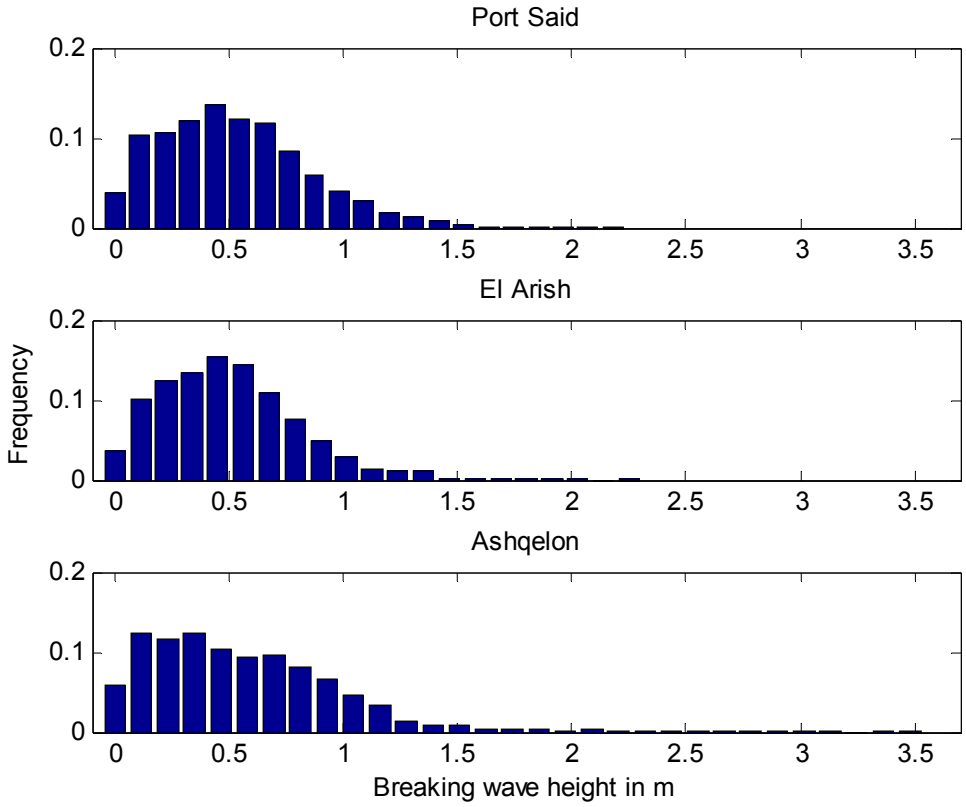

Figure 3.4 Frequency distribution of breaking wave heights for Port Said, El Arish, and Asqelon.

Table 3.5 Maximum breaking wave height, mean average breaking wave height, and frequency of occurrence of breaking wave height equal to or greater than 1m.

	Hmax (m)	Haverage (m)	H>1
Port Said	2.18	0.52	8.5
El Arish	2.25	0.50	6.4
Ashqelon	3.48	0.56	12.8

4. Longshore sediment transport

4.1 Calculations of Transport Rates

Wave-induced longshore sediment transport is caused by waves approaching the shore with an oblique angle to the shore. Breaking of waves causes turbulence and nearshore currents. The turbulence mobilizes sediment and the currents transport the sediment. The longshore sediment transport usually varies along a coastal stretch due to variations in wave climate, bathymetry, presence of coastal structures, etc (Larson and Hanson, 1992).

If a coastline is close to equilibrium there is no large shoreline change over time and the transport gradients between stretches along the shoreline approaches zero, if a large time scale is considered. However, there can be seasonal variations in the longshore sediment transport, since different angle sectors of approaching waves can predominate at different times of the season.

Waves approaching the shore with an oblique angle can be resolved into two components; shore-normal component and an alongshore component. The alongshore component of the wave power can be calculated by applying the expression for the longshore component of wave energy flux power (P_l) given by:

$$P_l = \frac{\rho g}{16} H_b^2 C_{g,b} \sin(2\alpha_b) \qquad (4\text{-}1)$$

where g is the acceleration due to gravity, ρ is the density of water, H_b is the wave height at breaking, $C_{g,b}$ is the group velocity at breaking and the α_b is the angle of the breaking waves to the shore normal.

The potential longshore transport rate (Q) in m^3/s is calculated from:

$$Q = \frac{K}{g(\rho_s - \rho)(1-n)} P_l \qquad (4\text{-}2)$$

where ρ_s is the density of the sediment grains, n is the void space between the particles and K is a transport coefficient.

The empirical coefficient K is site specific and can be calibrated to take the local conditions into consideration. When significant wave height is used for the breaking waves a K value of 0.39 can be used as a starting value. Instead, if the root-mean-square (rms) wave height is employed a K-value of 0.77 is recommended. However, the site specific value of K after calibration is typically in the range of 0.2-1.0 (CEM, part 3, 2002; Larson and Hanson, 1992).

The wave heights H_s and H_{m0} are approximately equal when irregular wave profiles are sinusoidal in shape. However as the depth becomes shallower and the waves are shoaling when approaching the beach, the waves start to become nonlinear and peaked in shape. The

H_s and H_{m0} wave heights are within 10 percent of each other if the depth is greater than or equal to (CEM, part 3, 2002):

$$h \geq 0.0975 T_P^2 \qquad (4\text{-}3)$$

other parameter values that were used in the present calculation of the longshore sediment transport is n=0.4, ρ_s =2650 kg/m^3,and ρ =1025kg/m^3, which is the density of water in the Mediterranean Sea.

The transport formula yields the potential rate and in reality it is common that the transport rate is lower than what the formula predicts. This can be due to a combination of different factors. Some important factors that influence the transport rate are:

- Shortage of available material to be transported
- Properties of the material
- Appearance of coastal obstructions as groins, jetties, breakwaters, submarine canyons, etc that can slow down or completely block the longshore sediment transport rate (CEM, part 3, 2002).

The breaking wave height has a nonlinear influence in the transport equation. If the wave heights, for example, have a Rayleigh distribution and the waves have the same period the transport rate using the distribution of wave height would be 1.53 times larger than computed using only the band-average wave height (CEM part 3, 2002).

Once Q is calculated for each wave in the time series that approaches the shore. To determine the net longshore sediment transport ($Q_{l,NET}$) equation (4.4) was used. Every Q value is included with sign, and by summing them all together it is possible to see in which longshore direction the sediment is transported. A positive $Q_{l,NET}$ indicates a movement of the sediments to the right and in the case of a negative $Q_{l,NET}$ the predominant direction is to the left. There is also the special case when $Q_{l,NET}$ becomes zero and in this case there is no net movement of sediment along the shore.

$$Q_{l,NET} = \frac{\sum_{1}^{i} Q}{i} \qquad (4\text{-}4)$$

The gross transport rate ($Q_{l,GROSS}$) is given by:

$$Q_{l,GROSS} = \frac{\sum_{1}^{i} |Q|}{i} \qquad (4\text{-}5)$$

where i is the number of input values of waves or wind (if the waves were calculated from the wind). A transport rate Q will be generated with the same duration as its input value. In the case of wind the duration is one hour, the transport rate Q also has a duration of one hour, i.e., one single Q value is representative for the conditions prevailing in one hour.

By setting i equal to the number of the input data instead of the number of Q values, also calm conditions when there is no transport of sediments will be taken into consideration. In this way $Q_{l,NET}$ and $Q_{l,GROSS}$ become representative average values for the net and gross

transport rates, respectively. The obtained cumulative transport rates were divided by number of wave observations to give an average transport rate for the entire series (see equations 4.4 and 4.5). The average $Q_{l,NET}$ and $Q_{l,GROSS}$ were then multiplied by a conversion factor of $3600 \cdot 24 \cdot 365$ to obtain the transport rate in m^3/year.This method was preferred over summing of all $Q_{l,NET}$ values and $Q_{l,GROSS}$ values, as the data gaps in the wind file would cause the magnitude of the annual transport rates to be underestimated. The wind file with the gaps of input data filled with adjacent values to get a representative year, could also have been utilized. However this method was not preferred as some input data period can get too large influence since they occur more than once in such a file.

When considering shoreline change the gradients of the sediment transport rate along the coastline has to be taken in consideration. For example, areas of convergent transport may correspond to a sediment accretion area, whereas areas of divergent transport may correspond to a sediment source (or erosion if the area is not a source). As long as there is an unlimited sediment source, a shoreline's response to long sediment transport should be dependent on gradients in transport along the coast rather than magnitudes of transport (CEM, part 3, 2002).

Transport rates calculated from wave data

Using the wave time series as input data to a computer program, the resulting transport rates along six stretches along the Sinai Peninsula were calculated, using a transport coefficient, K of 0.39 (see figure, 4.1). However, because the waves are measured at nearshore condition in the vicinity of Port Said, they are not representative for stretches, which differs greatly to the shoreline orientation present at Port Said. Figure 4.3 shows the offshore wave climate calculated from the measured nearshore waves. The waves are brought back to offshore conditions using Snell's law and the wave energy flux conservation equation. Also, using wind data, the offshore wave condition is calculated at Port Said, El Arish, and Ashqelon. By comparing the three wind-generated offshore wave conditions it is apparent that, the offshore wave conditions generated from measured nearshore waves is partly affected by shoreline orientation at Port Said. In other words, there are waves in the offshore wave conditions at El Arish and Ashqelon generated from winds that cannot be represented by the offshore wave condition at Port Said generated from the nearshore waves. This is further illustrated in figures 2.6, 2.8, 2.9 and 2.10. Therefore, it was decided to make the simulation using wind data to generate waves for each individual shoreline segment.

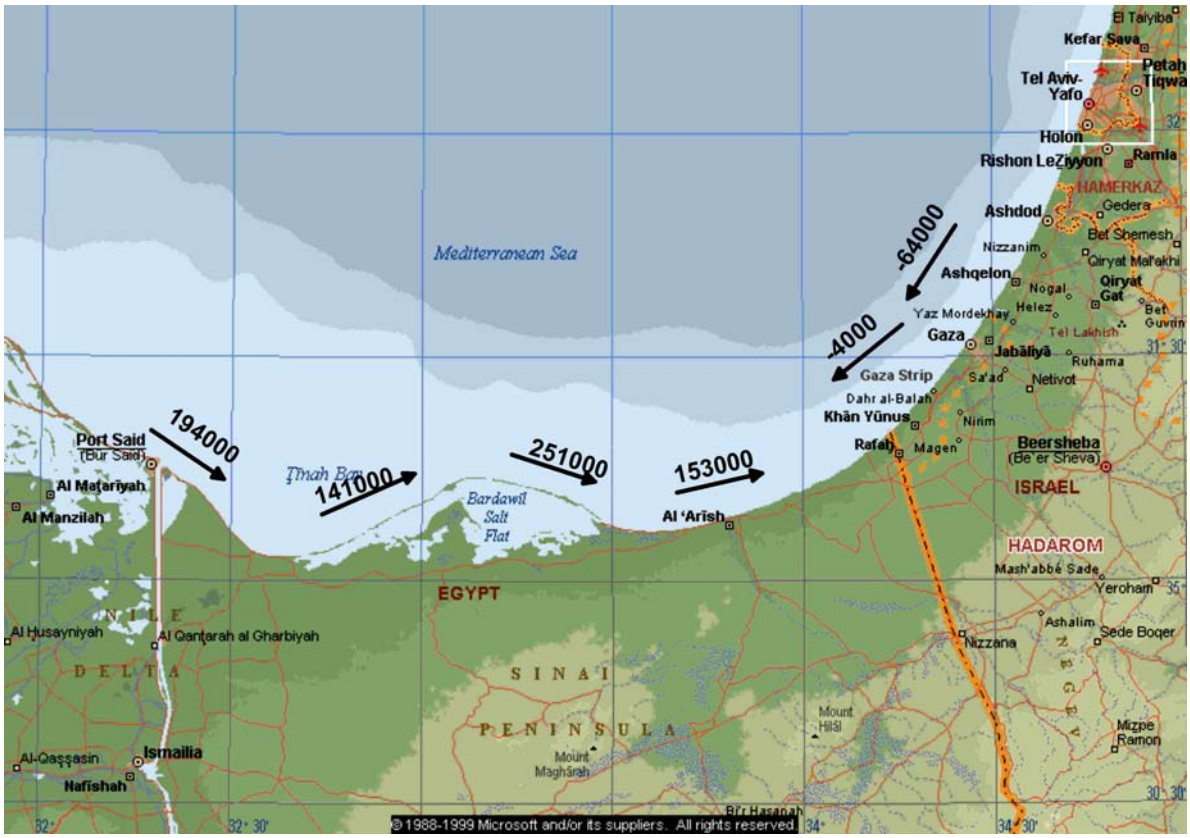

Figure 4.1 Transport rates [m^3/y] calculated from nearshore measured wave data.

Transport rates calculated from wind data

Since the measured waves are used for calculating the transport rate at Port Said along the stretch where the wave gage is located, the obtained transport rate utilizing waves as input data is considered to be close to the actual transport rate at this stretch. The model was therefore calibrated adjusting the transport coefficient, *K* (equation 4.2) such that the transport rate calculated from wind data at the Port Said shoreline stretch (34^o) was equal to the transport rate calculated from measured waves for the same stretch, at a *K* value of 0.57 agreement was reached. This *K*-value was than keep constant and utilized to calculate the transport rates for the other six stretches. The calculated net transport rates for different segments are shown in figure 4.2. As seen in the figure, the net volume of sediments transported alongshore changes from 194,000 m^3/year to 40,000 m^3/year from Port Said to the El Bardawil lagoon bulge. This indicates that Tinah Bay acts as a local accretion area. Farther to the east along the coast, the volume of net transport rate rises again to 258,000 m^3/year which shows that the sediment is being provided from the shore along the El Bardawil bulge creating erosion in this part of the coastline. Also, it can be concluded that sediment accumulates along the west stretch of El Arish shoreline since the volume of incoming sediments exceeds the outgoing volume. This area, where El Arish Power Plant and El Arish Harbor are located, is of particular interest in the present study. The transport rate at the El Arish stretch was estimated to be 164,000 m^3/year. From the El Arish coastline towards the east the net sediment transport rate increases to 178,000 m^3/year. The obtained pattern of sediment transport rate and direction is in agreement with the result of studies by Inman (2002) and Frihy and Lofty (1997). According to our mathematical modeling, a nodal point appears at Ashqelon where the direction of sediment transport rate changes. Inman (2002)

estimated the boundary of the littoral cell to be at Akko further to the east. Moving along the coast towards Ashqelon, the shoreline orientation changes such that the waves no longer approach the shoreline with the predominant angle of approach. As the waves predominantly approach the shoreline almost parallel to the shore normal, the magnitude of eastward sediment transport decreases.

Another interesting phenomenon to consider in the figure is the shadowing effect of the Damietta promontory. This is manifested by the difference in the volume of net sediment transport at Port Said and west of El Arish. At these two locations, although the angle of shoreline orientation is almost the same, the net transport rate to the west of El Arish is 64,000 m^3/year greater than the net transport rate at Port Said. This further emphasizes that some waves are shadowed west of Port Said and cannot reach the shoreline here. However, part of the magnitude difference is also caused by the increased fetches to the east. The difference in fetch lengths between the three different wave climate compartments is only accounted for in the modeling utilizing winds as source data.

The large-scale sediment transport rates calculated from wind (figure 4.2) and waves (figure 4.1) turned out to be more similar than first was suspected, and the methods are both able to capture the regional transport pattern along the Sinai Peninsula.

The mathematical model shows the general patterns, but is not able to interpret accretion-erosion areas that are caused by hard structures that perturb the littoral drift, i.e., the change from accretion to erosion caused by the west breakwater at El Arish Harbor.

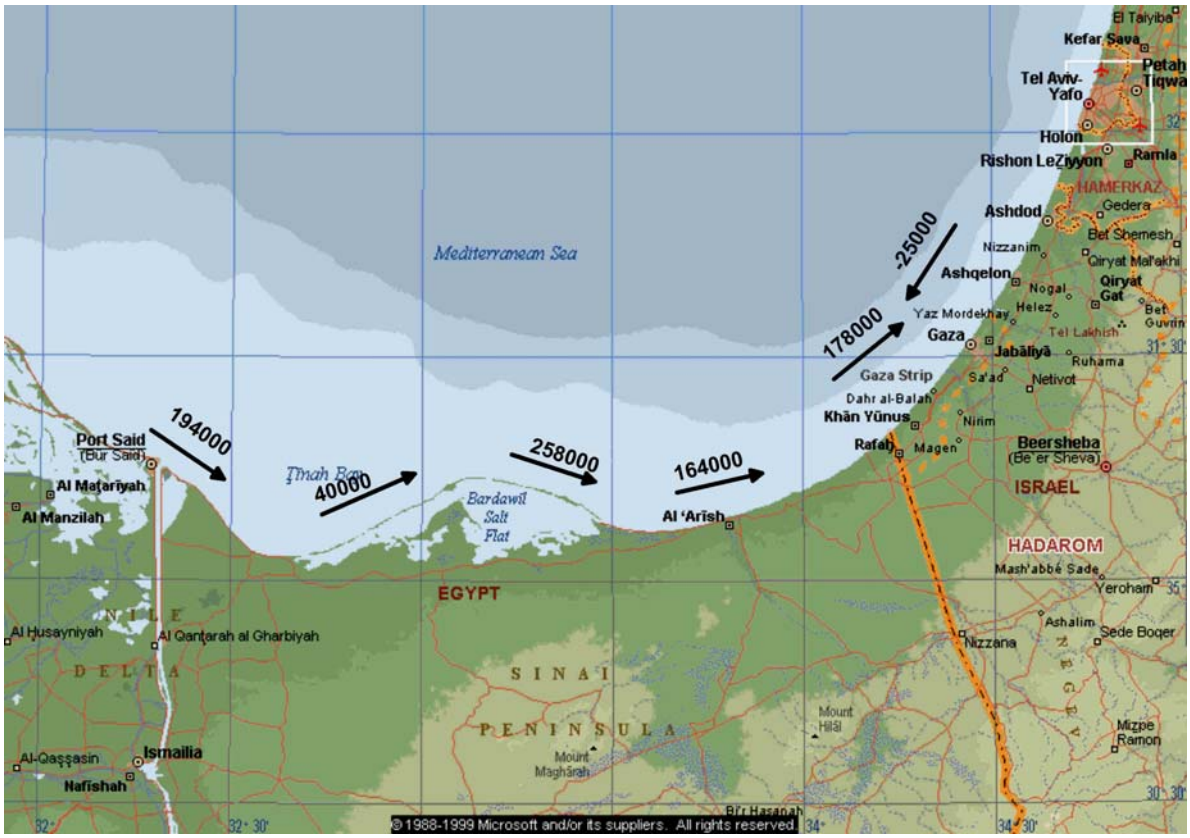

Figure 4.2 Volume and direction of net transport rates [m^3/y] along the Sinai northern coast.

Gross transport rates can be of interest to investigate at the inlet of the cooling water intake basin as the sediment can settle out in the intake basin regardless of the direction of

movement. Dredging inside the intake basin creates a local depression in the bottom topography that can act as a sediment trap. The gross transport rate at the intake basin was determined to be 453,000 m^3/year.

5. Modeling Shoreline Evolution

5.1 Introduction to Beach Change Modeling

Numerical models can be used as supplemental tools in the decision-making process to evaluate the effects of different proposed coastal engineering measures. In general it is of interest to make a preliminary evaluation of potential changes that are likely to happen in response to implementation of a particular coastal engineering practice. In this context, numerical models facilitate forecast of the effect of the different alternative measures and from changes in wave conditions. By applying numerical models in shoreline change modeling, it is possible to account for more complex conditions, such as temporally and/or spatially varying wave conditions and systems with multiple structures.

Shoreline change or shoreline response models simulate changes in position of shoreline due to wave action within specified boundaries. The shoreline change models perform best when a perturbation occurs to a shoreline that is in equilibrium. The perturbation can be caused by the construction of hard coastal structures, for example, a groin or a jetty. The disturbance can also be a result of sand mining, placement of beach fills, and/or similar soft coastal engineering practices.

Immediately, after the completion of a project that causes perturbation to a shoreline, the system is so far from equilibrium that, at this time changes by longshore sediment transport usually dominates over storms and seasonal variations. Under such conditions even simulations performed over a short time interval can give reliable results. However, as the beach approaches a new equilibrium, it becomes more important with longer simulation intervals to prohibit overly great influences from seasonal variations in the simulation.

The models are usually calibrated and validated utilizing historical trends captured from satellite images, aerial photos and/or from different surveying techniques and from estimates of sediment transport rates. To be able to get good results from the model it is necessary to have reliable input data against which the model can be calibrated with representative calibration parameters for the specific coastal stretch of concern (CEM, part 3, 2002; Hanson and Kraus, 1989) .

5.2 Shoreline Response Modeling

GENESIS (GENEralized model for SImulating Shoreline change) is a one-line numerical model developed by Hanson and Kraus (1989) to examine shoreline change at costal engineering projects. GENESIS calculates shoreline change due to spatial and temporal gradients in sediment transport generated by breaking waves. Pelnard-Considere (1956) formulated and experimentally verified the mathematical framework used in GENESIS. The description of GENESIS given here is not all-embracing. For a more detailed description the technical manual for GENESIS can be consulted (Hanson and Kraus, 1989). However, a short description of the model encompassing the parts that are important to this project is presented below.

The change in volume ΔV for a shoreline segment is determined by the net amount of sand that enters or exits the segment from its four sides.

$$\Delta V = \Delta x \, \Delta y \, (D_B + D_C) \qquad (5\text{-}1)$$

where Δx is the length of the shoreline segment, Δy is the change in shoreline position, D_B is berm height and D_C is depth of closure. Kraus *et al.,* (1998) defined the offshore depth of closure for a given time interval as the most landward depth seaward of which there is no significant change in bottom elevation and no significant net sediment transport between the nearshore and the offshore. Hallermeier derived an expression for the depth of closure:

$$D_C = 2.28 H_C - 68.5 \left(\frac{H_C^2}{g T_C^2} \right) \qquad (5\text{-}2)$$

where H_C is the local significant wave height exceeded 12hr in a particular time interval (one year in this study) and T_C is the wave period associated with H_C.

One contribution to the volume change ΔV occurs when there is a difference in the sand volume transported in and out from a cell in the direction of longshore sediment transport. This longshore sand volume change can be expressed by equation 5.3. A cell is the compartment unit that GENESIS works with for sediment budgets. Sediment motion occurs uniformly within the elevation limitations set by the depth of closure and berm height.

$$\Delta Q \, \Delta t = \left(\frac{\partial Q}{\partial x} \right) \Delta x \, \Delta t \qquad (5\text{-}3)$$

Another type of contribution to the volume change is from sand sources or sinks, added or removed within the line of the active profile, named line sources or sinks. This type of sources and sinks is given in volume change per unit width $\pm q$. Examples of linear sources, are beach nourishment, river outlets and land slides, whereas sand removal by sand mining and dredging of the beach are examples of linear sinks. The total volume change from these linear sources and sinks is given by:

$$q \, \Delta x \, \Delta t \qquad (5\text{-}4)$$

GENESIS does not account for the wave-generated cross-shore transport through the q term. Instead, cross-sectional source of material can be represented by a positive beach fill, whereas a loss of material can be input as a negative beach fill. Summation of the contributions of the different components of the volume change given by equations 5.3 and 5.4 yield the total volume change as expressed by equation 5.5. By equating these two expressions it is possible to derive the expression for conservation of sand volume as follows:

$$\Delta V = -\Delta x \, \Delta y \, (D_B + D_C) = \left(\frac{\partial Q}{\partial x} \right) \Delta x \, \Delta t \pm q \, \Delta x \, \Delta t \qquad (5\text{-}5)$$

By rearranging the equation 5.5 and taking the limit when Δt approaches 0, the following equation is obtained:

$$\frac{\partial y}{\partial t}+\frac{1}{\left(D_B+D_C\right)}\left[\frac{\partial Q}{\partial x}\pm q\right]=0 \qquad (5\text{-}6)$$

To be able to solve equation 5.6 an initial shoreline for the whole reach modeled, boundary conditions, and values of Q, q, D_C, and D_B must to be specified.

To calculate the longshore transport GENESIS uses a semi-empirical predictive equation:

$$Q=H_b^2\,C_{g,b}\left[a_1\sin 2\theta_{b,s}-a_2\cos\theta_{b,s}\frac{\partial H}{\partial x}\right]_b \qquad (5\text{-}7)$$

where H_b is the wave height at breaking, $C_{g,b}$ is the group speed at breaking, $\theta_{b,s}$ is the angle of breaking waves to the local shoreline, and x is the longshore direction.

The non-dimensional parameters a_1 and a_2 are given by:

$$a_1=\frac{K_1}{16\left(\frac{\rho_s}{\rho}-1\right)\left(1-n\right)\left(1.416\right)^{5/2}} \qquad (5\text{-}8)$$

$$a_2=\frac{K_2}{8\left(\frac{\rho_s}{\rho}-1\right)\left(1-n\right)\tan\beta\left(1.416\right)^{7/2}} \qquad (5\text{-}9)$$

where K_1 and K_2 are empirical calibration coefficients, ρ_s is the density of sand (taken to be 2650 kg/m^3), ρ is the density of the water (1030 kg/m^3), n is the porosity of the sand (0.4), and $\tan\beta$ is the average bottom slope from the shoreline to the depth of closure.

The first part of equation 5.7 is responsible for the longshore sand transport caused by waves approaching the beach with an oblique angle. This expression includes the K_1 coefficient, which is influential on the sand transport rate and sets the response time scale of the simulated shoreline. The coefficient K_1 should be adjusted in the calibration process to get a good agreement with the measured shoreline and known transport rates in the area. The second part of the equation accounts for the effect of diffraction, and this part of the equation is usually less influential than the first part, but improves the model result where diffraction is important as in the case where long coastal structure occurs. To obtain suitable curvature in the vicinity of diffracting structures the K_2 coefficient can be adjusted.

GENESIS has been applied to shoreline stretch lengths from 1 to hundreds of km, with grid resolution typically from 10 to 100 m. And the simulation intervals span typically around 1 – 20 years, with repeated wave condition input every 30 min to 6 hr.

In this project GENESIS95 V.3 is utilized. The user friendliness and variety of coastal structures accounted for in GENESIS have increased in the more recent versions of the program. The software is capable of simulating the effect of groins, jetties, breakwaters, beach nourishment, seawalls, and detached breakwaters in many different combinations. Groins, jetties and breakwaters can be diffracting or non-diffracting. T-groins, Y-groins and

spur groins can be simulated by combining a detached breakwater with diffracting groins. Permeability of groins and bypassing operations can be simulated. Waves can be provided in the offshore or as breaking waves, if an external wave refraction program is used. The wave height, wave direction, and wave period can vary both in time and space. In situations where multiple wave sources occur, GENESIS can have multiple wave trains as wave input.

In addition to the limitations set by the assumptions made in the mathematical frame work behind GENESIS, the program also involves some additional simplifications. GENESIS cannot simulate the effects of wave reflection from structures and GENESIS V.3 used in this study cannot simulate the effects of a tombolo formation behind a breakwater, but this is represented in later versions. This happens the when continuous accretion causes a salient to extend seaward and reach the breakwater. The material transported is assumed to be sand with a uniform grain size over the entire simulated stretch. Areas that differ greatly regarding grain size will give unreliable results. The berm height and closure depth are also assumed to be constant over the entire stretch. A solution to this limitation could be to split up the simulated stretch into sub stretches with site specific differences in input parameters.

If the beach is in equilibrium and no perturbation occurs during the simulation period it will be difficult to determine the most appropriate K_1-value through model calibration. The model might perform poorly in the case of large tidal difference, beach change occurring inside inlets, undermining of structures, and, finally, great influence of net cross-shore sediment transport rate, which can be caused by frequent occurrence of large storms.

5.3 Model Calibration and validation

The two main calibration parameters are K_1 and K_2. Other parameters that the model can be calibrated with are wave height, wave angle change factor, smoothing window, grain size, berm height, and depth of closure. However, many of the parameters mentioned above can be determined, if the physical conditions at the beach are well examined, or at least the variation interval of them can be narrowed. When the shoreline predicted by GENESIS and the measured shoreline have a good agreement the model can be verified by holding the calibration parameter values constant and applying the model to a new simulation in a time interval different than the one used for calibration.

Calibration and verification of the model at El Arish Power plant

The calibration at the power plant was performed for a 16-month interval between 1995-01-01 and 1996-04-30. The breakwaters at the power plant were assumed to have been constructed at 1995-01-01. A shoreline surveyed in 1992, before the construction of the power plant, was used as initial shoreline for this part of the project as no reliable shoreline measured closer in time to the construction date was available. The initial shoreline is visible as the black line and the measured shoreline is pink in the GENESIS simulation window shown in figure 5.1. To simulate the effect of the western breakwater, a 195 m long groin was added, which is red-brown in the figure. Two seawalls were applied, one at the power plant intake basin and the other one at the effluent discharger. The seawall at the intake basin is added to represent the stable shoreline inside the harbor and the seawall at the discharger is added to simulate the effect of stones and boulders and the hard structure of the discharger.

There are two types of boundary conditions commonly used in GENESIS, that is “pinned beach” condition and “gated” condition. The boundary can be assumed to be pinned in places were no change in the shoreline position occurs. In other words nodal points can be utilized as pinned beach boundary condition. A gated boundary condition may be applied when shoreline position at the boundary can be changed as a result of some preferential gain or loss of littoral material, for example, in the case of long jetties, long groins, and inlet channels. Additionally, if the net sediment transport rate is known at a particular point at the beach, that point can be set as the boundary for the simulated stretch. In such cases the model must be calibrated so that the calculated value for the net sediment transport rate at the defined boundary corresponds to the known net transport rate.

Unfortunately, the shoreline stretches surveyed by the Coastal Research Institute and Suez Channel Survey at the power plant were too short (2.88 km) and did not contain any of these preferable boundary conditions. The entire surveyed stretch provided on the chart was modeled and even though no estimate of the net transport rate was available at the start and end point, moving boundaries were applied. In other words, the amount of seaward and/or landward translation of shoreline position during the simulation run were specified at the two ends of the stretch. This was done by calculating the difference between shoreline positions in the initial and measured shoreline for the first and final cells respectively. As different shorelines are modeled in the calibration and verification simulations, the value of the boundary movement varies accordingly for the calibration and the verification, see table 5.1 and figures 5.1 and 5.2.

Many simulations were performed to calibrate and understand how the input parameters affected the simulation results. The parameter values that generated the best agreement between the measured shoreline and the calculated final shoreline are presented in table 5.1 and 5.2. The closure depth, D_c were calculated to 4.6m using equation 5.2. However, to get the sediment budget calculation right during the calibration process for the power plan, the closure depth were decreased.

The value of the time step in hours, Δt is the step with which the model precedes forward in time, a small time step will increase the run time and a too large value may result in a loss in accuracy of the shoreline position. On the otherhand a too small time step may also cause numerical instability. In the present simulations a time step of 6 hours was used. To provide the model with correct wave data for every time step a wave data file was generated, providing the model with wave period, wave height, and wave angle every 6 hours.

The number of calculation cells in the smoothing window specifies the number of cells that will be used in the calculations of the shoreline orientation affecting the wave transformation for each cell. The calculated final shoreline can be seen in figure 5.1. By applying the simple sediment conservation calculations it was possible to get the right proportions of sand volumes on the updrift and downdrift side of the groin.

Calibration was also done by making changes to the wave parameters. This was done based on the fact that the wave data file was prepared for a period of time different than the period in which the model is calibrated and verified. Our one-year wave climate data file starts from June 1999 through June 2000. By trying to account for these small annual variations a good correspondence between the measured and calculated final shoreline was obtained. By keeping the changes fairly small the general trends in the wave climate that are the same over the years were not lost. Similarly, changes in the wave file between calibration and

verification can be justified for the same reason, because the wave conditions between the calibration and verification period most likely varied to some extent. The parameters values applied to the wave file for the calibration and verification period are presented in table 5.2.

The volumetric change between the final shoreline calculated with GENESIS and the initial shoreline gives a net accretion of 67,000 m^3 for the simulation period. This calculated sand volume can be compared with the volume of 70,800 m^3 between the initial and final measured shorelines, determined using equation 5.1. The mean absolute difference distance (called calibration/verification error in GENESIS) between the measured and calculated shoreline is 8.7m.

Table 5.1 Model settings and calibration and verification parameters for the El Arish power plant simulations.

	Calibration	Verification
Total number of cells	192	192
Value of time step	6h	6h
Number of calculation cells in smoothing window	40	40
Cell length	15m	15m
K_1	0.7	0.7
K_2	1.0	1.0
D_C closure depth	3.0m	3.0m
Grain size	0.2	0.2
D_B berm height	1.0	1.0
Boundary movement left boundary	33	43
Boundary movement right boundary	-47	13

Table 5.2 Calibration and verification parameters for the power plant simulation.

	Calibration	Verification
Value of time step for wave data	6h	6h
Wave height	1.4	1.4
Wave angle change amount	5	15
Wave angle change factor	1	1.03

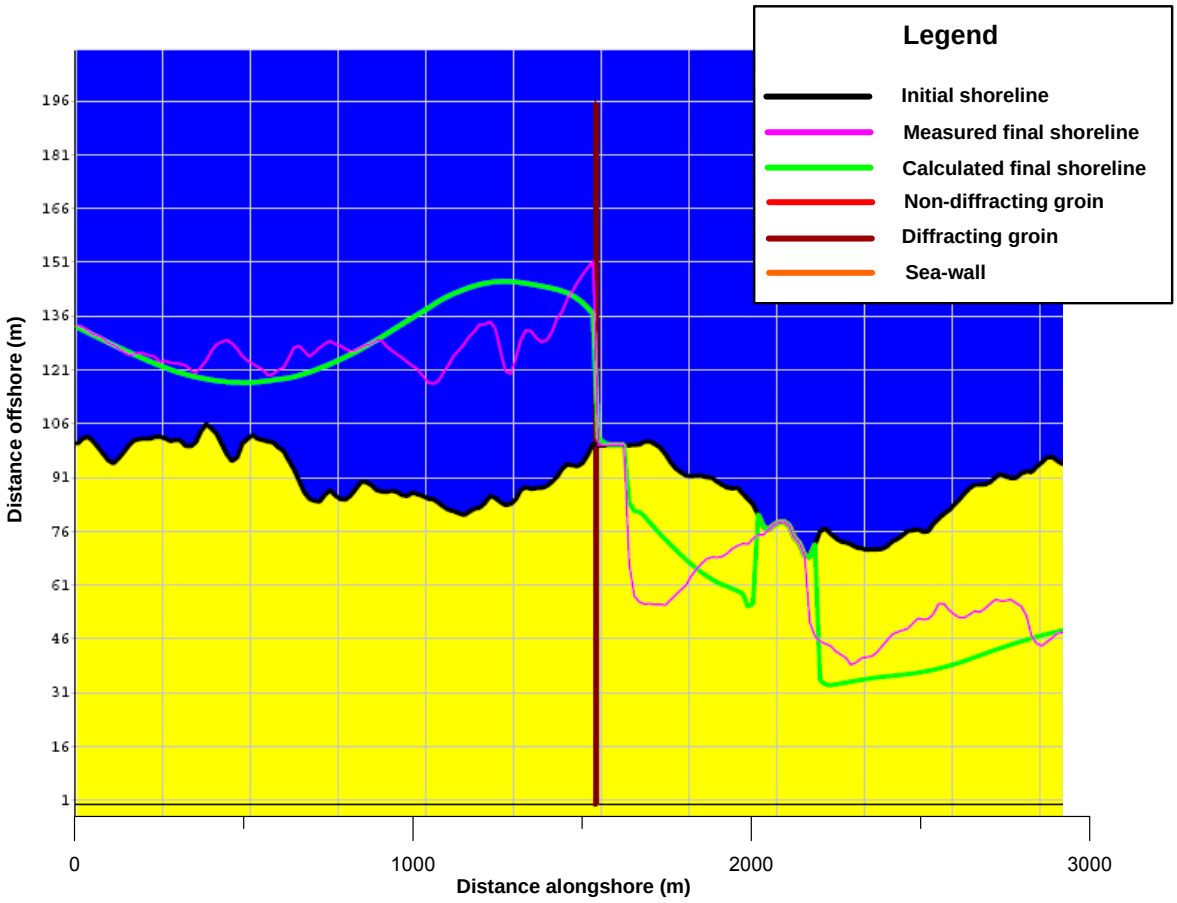

Figure 5.1 Simulated and measured final shorelines for the calibration of the model for El Arish power plant.

The verification period spans over a 25-month interval between 1996-04-30 and 1998-05-31. The parameter values are held the same as for the calibration simulation. A fairly good agreement was obtained between the measured shoreline and the calculated, see figure 5.2. The calculated volumetric change gives a net accretion of 261,000 m^3 for the period. This sand volume calculated can be compared with the volume of 222,300 m^3 between the measured initial and shorelines, calculated using equation 5.1.

The mean absolute difference between the measured and calculated shorelines in the verification run is 11m. The worse fit, as compared with calibration, is mainly because the shorelines are far apart in the accretion area updrift the breakwater. It was preferred to have a good correspondence between the shorelines in the immediate vicinity of the groin resulting in an increase in the difference between the position of simulated and measured shorelines over all. However, looking at the measured shoreline from May 1998, it seems that some sand removal might have taken place in the accretion area near the breakwater as the shoreline position does not advance as much farther to the west in the accretion part, see figure 5.2.

During the calibration the calculated bypassing rates at the breakwater are lower than during the verification period. The bypassing rate for the calibration period was calculated to be 136,000 m^3/year, which can be compared to the bypassing rate of 228,000 m^3/year for the first year and 271,000 m^3/year for the second year of the verification simulation. The increase in the bypassing rate at the cooling water intake basin, is a direct effect of the area west of the breakwater becoming almost fully accreted. Less material will be able to accumulate at the groin. Instead, more sand material will bypass the groin and deposit in the intake channel and the intake basin for the power plant located east of the groin. All the material that moves due

to wave action and bypasses the groin is assumed to be trapped in the intake channel. The sand that is trapped by the intake channel is continuously dredged, pumped and disposed of east of the intake basin. As the volume of sediment trapped by the channel increases the dredging efforts has to be intensified. Thus, more material will be provided to the area east of the breakwater and the erosion ceases. During the verification period a small accretion trend is detectable east of the groin implying that erosion is no longer the major problem in the area immediately downdrift of the power plant. Rather, the problem is the dredging that has to take place to keep the intake channel free from sediment.

The result from the model simulations of power plant impact on the beach should be assessed keeping its different weaknesses in mind. Uncertainty regarding the boundaries and that the wave data do not correspond to the actual years simulated has to be considered when the result is assessed.

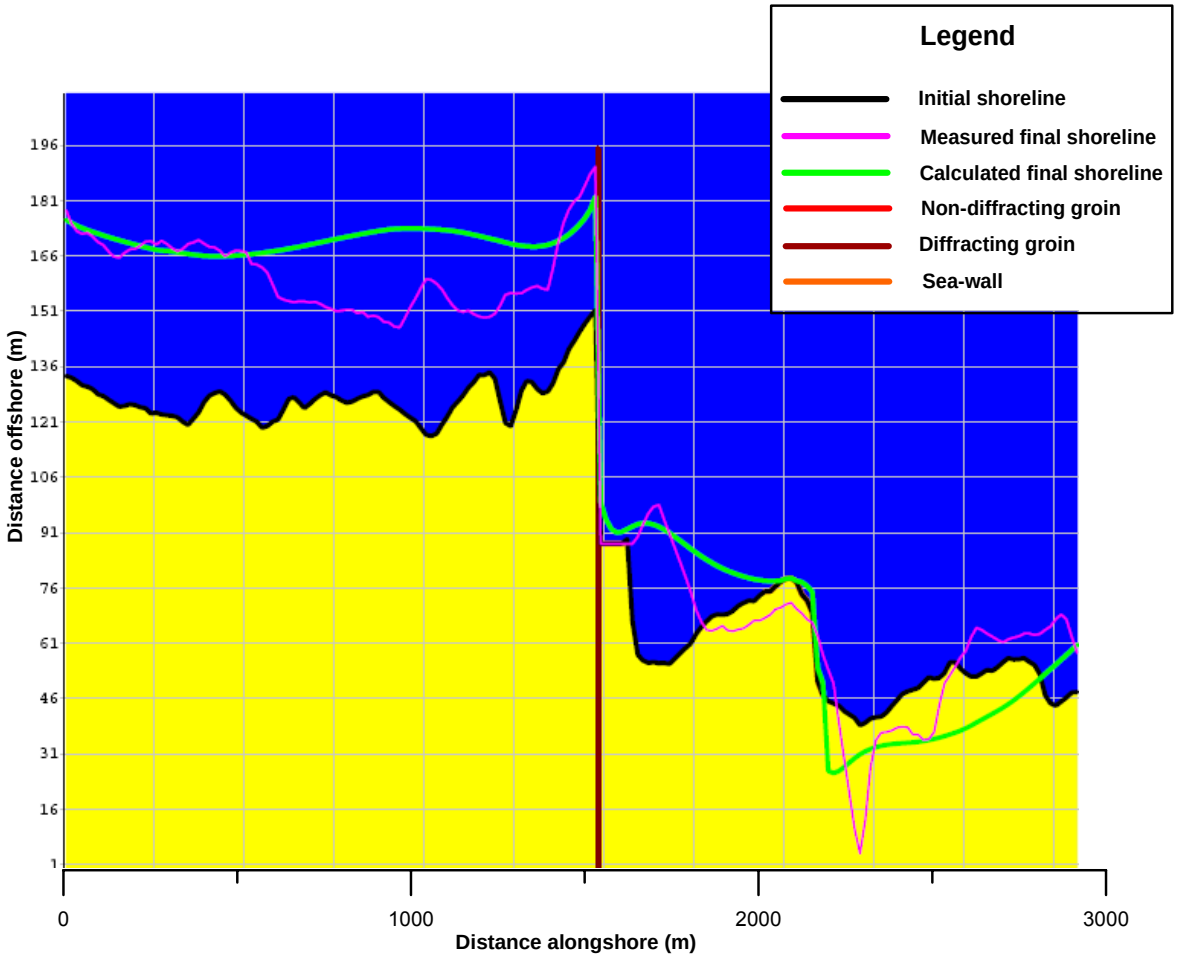

Figure 5.2 Simulated and measured final shoreline for verification of the model for El Arish power plant.

Sensitivity testing for the model at El Arish Power Plant

Sensitivity testing refers to the process of examining changes in the output of a model resulting from intentional changes in the input parameters. If large variations in the output from the model are caused by a small change in the input, calculated results will depend too greatly on the quality of the verification, which increases the uncertainty of the model predictions. If the model is too sensitive to small changes in input values, the range of

possible predictions by the model will be too wide and it will not generate any useful information (Hanson and Kraus, 1989).

The sensitivity test was preformed in a systematic manner, by applying a change to only one parameter at a time for each simulation run. Figure 5.3 shows how the verification shoreline responds to the different changes in parameter values for K_1, K_2, grain size, closure depth, and berm height. Table 5.3 shows the changes in simulation result for the different input parameters.

Figure 5.4 illustrates how the verification shoreline responds to parameter changes concerning the wave climate. The wave height change factor, wave angle change factor, and wave angle change amount were modified and the values that these parameters were changed with are presented in table 5.3(see also tables 5.1 and 5.2 to examine how the values differed from the original calibrated parameter). Table 5.3 also shows the volume change induced by the parameter change.

To make comparison between the shoreline response due to the parameter change and the original verification shoreline possible, the original verification shoreline is also presented together with the shorelines simulated with the parameter changes in figures 5.3 and figure 5.4 .

The model did not show much sensitivity against small changes in the input parameters implying that the verification simulation could be considered as rather reliable.

Table 5.3 Sensitivity testing for different parameters as well as resulting volume change and a mean absolute difference distance between final measured shoreline and final calculated shoreline.

	parameter value	relative change ΔV/1 000 m^3	mean absolute difference distance (m)
Original parameter values		0	10,8
K_1	0.8	31	11,97
K_2	1.1	-3	10,75
Grain size	0.17 mm	-15	9,54
D_C closure depth	3.5 m	1	11,16
Wave height change factor	1.5	25	11,09
Wave angle change factor	1.0	2	11
Wave angle change amount	12	-4	10,5

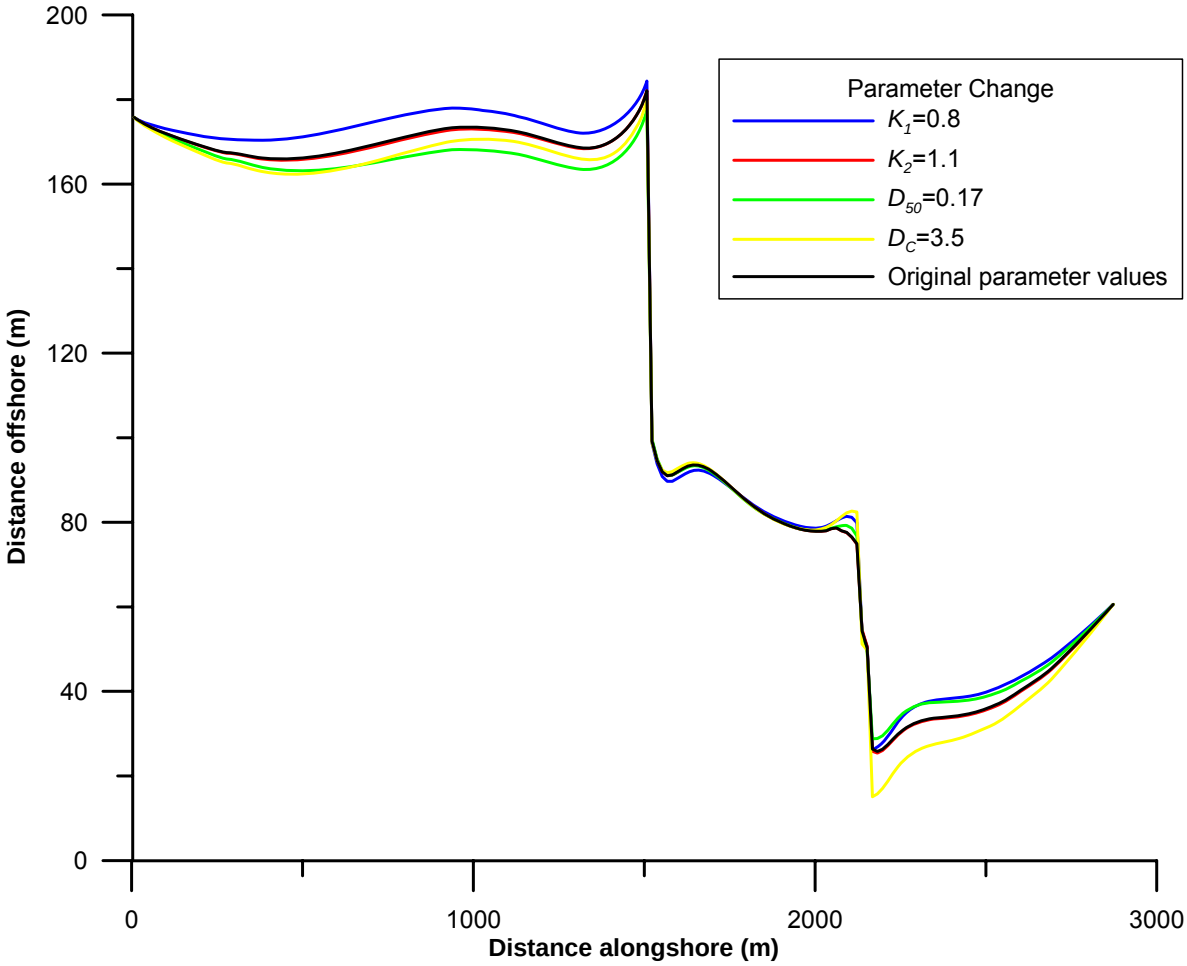

Figure 5.3 Results of sensitivity testing for El Arish power plant with regard to changes in calibration coefficients K_1 and K_2, median grain size D_{50}, and depth of closure D_C.

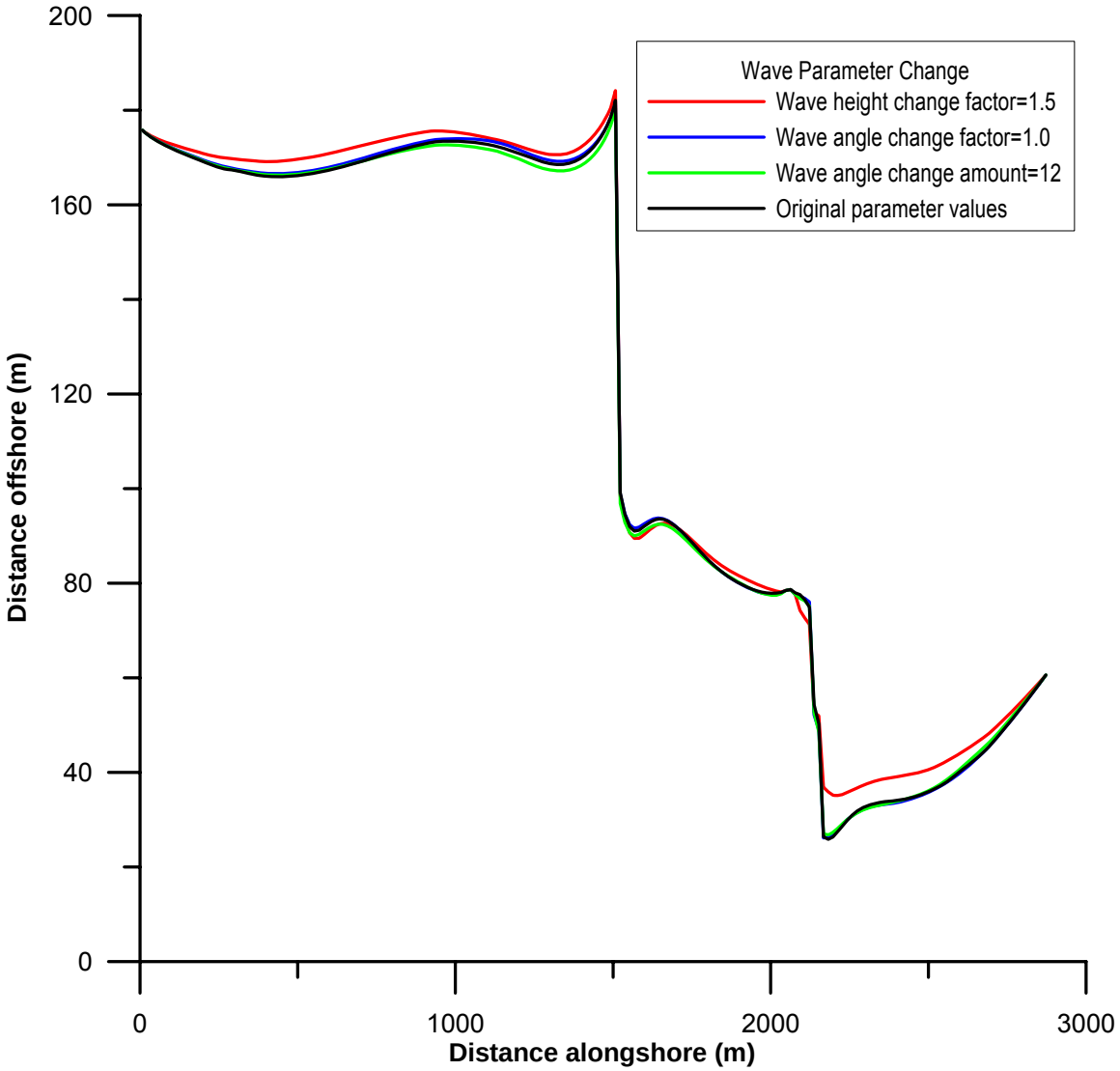

Figure 5.4 Results of sensitivity testing for El Arish Power Plant with regard to changes in wave parameters.

Calibration of model at El-Arish Harbor

El-Arish Harbor was modeled over a stretch of 10.5 km. The initial and final shoreline positions and configuration of coastal structures before and after the construction of the harbor were obtained from satellite images for 1973 and 2001. The model was run for a 17-year simulation period to quantify sediment transport rate and give an image of shoreline change over this stretch. This modeling effort was carried out to replicate the overall picture of the sediment transport along the El-Arish Harbor coastline.

After digitizing the satellite images, it was decided to apply a pinned beach boundary condition as two nodal points were identified to delineate the simulation stretch. The El-Arish harbor is located 3150 m from the western boundary. The stretch was divided into 150 cells, each 70 m long. Later on, it was realized that a longer stretch should have been used as the boundaries affected the calculated net transport rates. This conclusion was drawn as, throughout the simulation period, the net transport rates decreased as a result of local change in the shoreline orientation due to sediment accumulation. To minimize the effect of boundaries 30 cells and 20 cells with the same shoreline position in the west and east,

respectively, were added to the stretch (see figure 5.5). In this way, the number of cells was raised to 200 which is the maximum number of cells that could be simulated by the student version GENESIS v.3.

A sand budget was established using the two shorelines to understand the accretional/erosional behavior of the stretch. By so doing, a negative volumetric change of about 310,000 m^3 was calculated implying that, on the whole, erosion takes place along the stretch. The harbor was modeled as a 610 m long groin extending seaward. Furthermore, a groin field was introduced from cell 66 to 101. The lengths of the coastal structures were estimated on images obtained from Google earth.

However, the actual lengths of the groins were changed in the calibration process to obtain a better fit between the measured and calculated shorelines as well as volumetric calculations. In response to the vast sediment deficit after the placement of each groin the beach started to erode immediately downdrift of the newly constructed groin. In this way, the erosion has been transferred to the downcoast of the groin field. There were no data available with regard to the chronological order of the construction of the groins. Therefore, when modeling the shoreline it was assumed that the groins were constructed simultaneously.

Despite the great length of the breakwater that extends beyond the closure depth, it was modeled as a non-diffracting groin as it was not possible to use a combination of diffracting and non-diffracting structures in the simulation. Finally, similar to the case of the power plant intake basin a seawall was added east of the breakwater as the shoreline inside the harbor is stable. The mean absolute difference between the measured and calculated shoreline is 15.8 m. The resolution of the available satellite images were coarse which can cause inaccuracy affecting the shoreline position calculations Table 5.4 gives the calibration parameter values for the harbor.

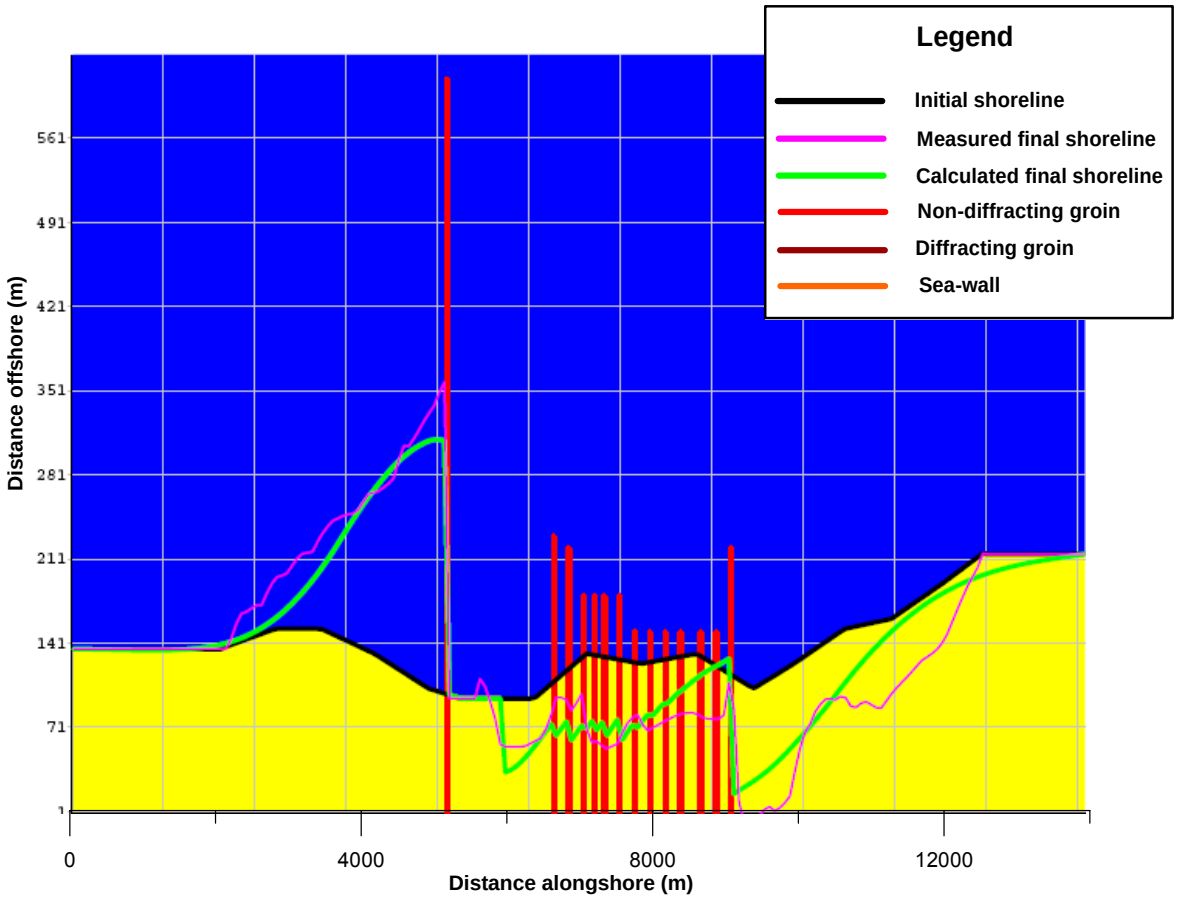

Figure 5.5 Simulated and measured final shoreline for the calibration of the model for El Arish Harbor.

Table 5.4 Calibration parameter values for the harbor

Number of cells	200
Value of time step	6hr
Number of calculation cells in smoothing window	21
Cell length	70
K_1	0.6
K_2	0.39
Depth of closure	4.5
Grain size	0.2
Berm height	2
Wave height change factor	1
Wave angle change factor	1
Wave angle change amount	6
Boundary movement left boundary	0
Boundary movement right boundary	0

Sensitivity testing of the model at El Arish Harbor

There was no verification shoreline available for the case of El Arish harbor. Instead of testing the model sensitivity in the verification simulation, it was examined in the calibration

simulation. Figure 5.6 shows how the calibration shoreline responds to the different changes in parameter values K_1, K_2, grain size, closure depth, and berm height and table 5.5 summarizes the changed values for the different input parameters.

The wave height change factor, wave angle change factor, and wave angle change amount were also modified (see figure 5.7). Table 5.5 shows the values that the parameters were changed to. To compare the shoreline response to the parameter change and the original calibration shoreline, the original calibration shoreline is also presented in figures 5.6 and 5.7 together with the shorelines simulated with the parameter changes.

The model did not show much sensitivity against small changes in input parameters implying that the calibration could be considered rather reliable.

Table 5.5 Sensitivity testing of parameter values as well as resulting volume change and mean absolute difference distance.

	parameter value	relative change ΔV (m^3)	mean absolute difference distance (m)
Original parameter values		0	15,8
K_1	0.7	300	15,6
K_2	0.49	-300	15,8
Grain size	0.17mm	300	16,9
DC closure depth	5.0m	-1300	16,7
Wave height change factor	1.1	3400	16,5
Wave angle change factor	1.1	-500	16,1
Wave angle change amount	3	2000	16,8

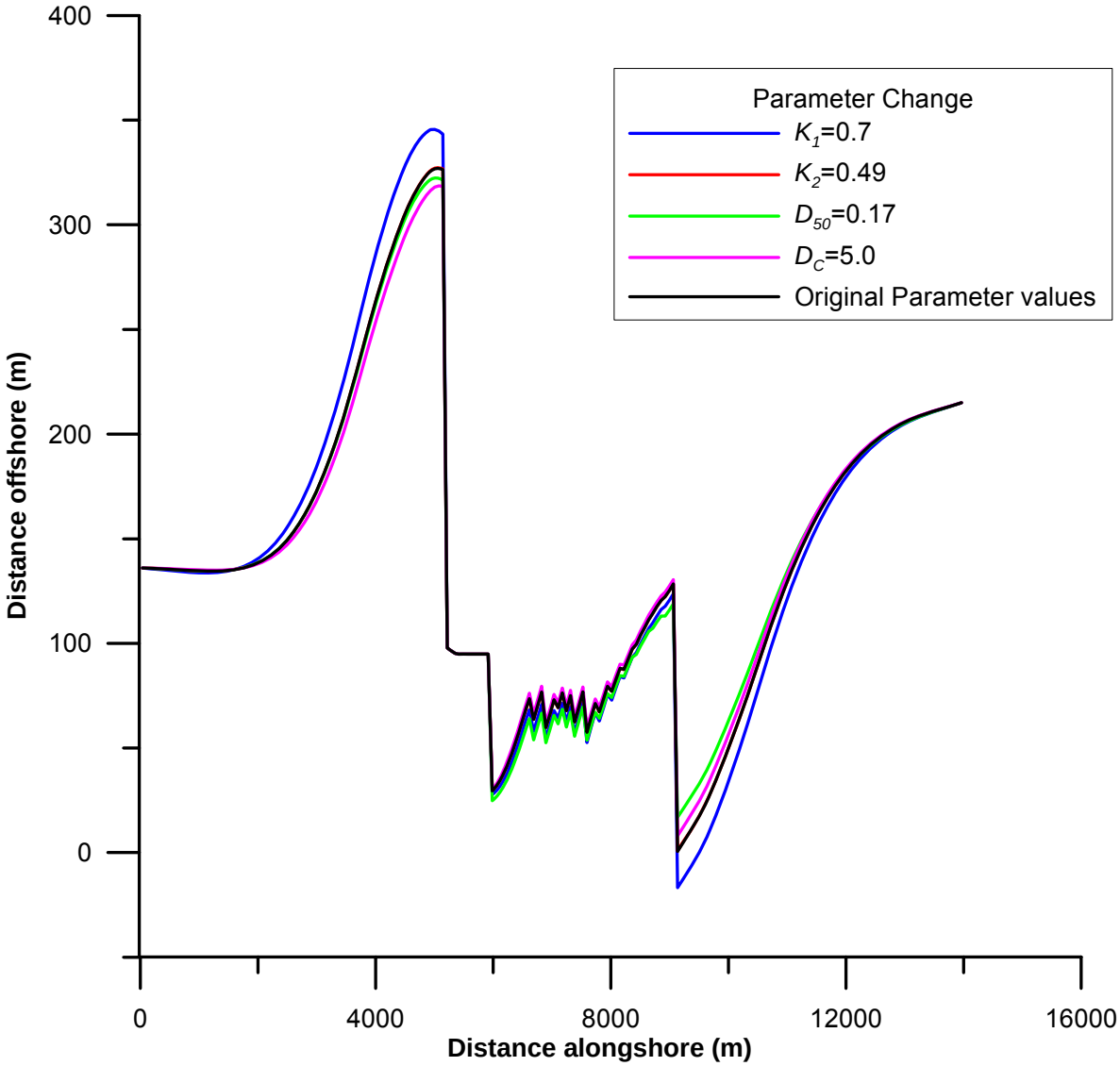

Figure 5.6 Results of sensitivity testing for El Arish harbor with regard to changes in calibration coefficients K_1 and K_2, median grain size D_{50}, and depth of closure D_C.

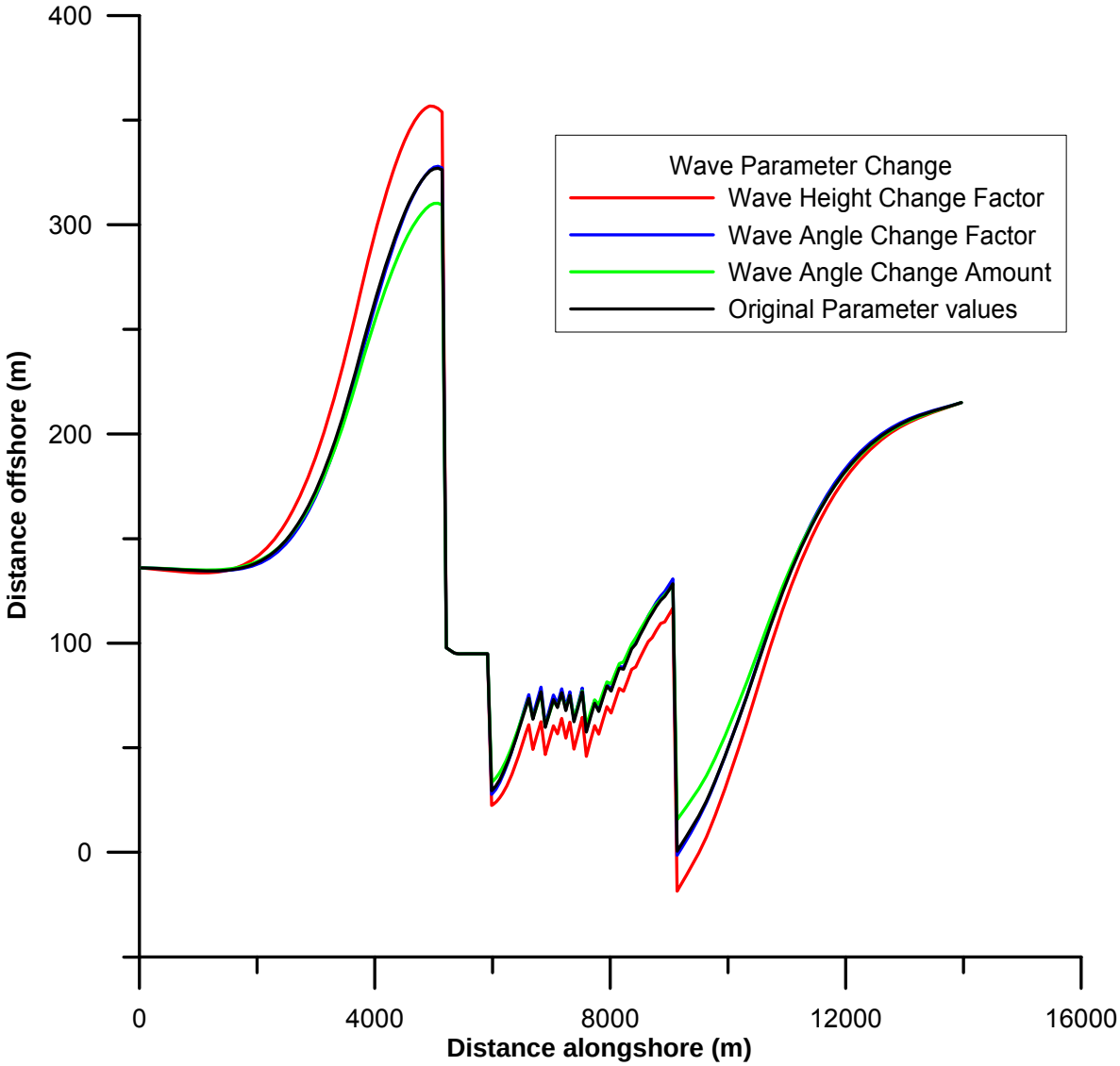

Figure 5.7 Results of sensitivity testing for El Arish Harbor with regard to changes in wave parameter.

6. Remedial measures to prevent erosion

6.1 Overview of typical solutions

A variety of structural and non-structural methods are available to the coastal engineer to tackle the problem of coastal erosion. Hard structures are constructed to prevent further erosion of a beach or to entrap littoral drift within a littoral cell by impeding the alongshore movement of sand. Several types of coastal structures may be used to stabilize an eroding beach. Coastal armoring structures, e.g. seawalls and revetments have been widely practiced to prevent the erosion of the upland. Typical coastal protection works that impede alongshore sand movement include seawalls, revetments, groins, jetties, and detached breakwaters. The presence of coastal defense structures is almost always accompanied by accelerated downcoast erosion. In contrast, soft mitigative solutions such as artificial nourishment of beaches can serve to compensate for the sediment lost from the littoral system. In this section, various strategies and methods for dealing with erosion, possibly applicable to the Sinai northern coastline, are discussed based on descriptions provided in Coastal Processes with Engineering Applications (Dean and Dalrymple, 2002).

Seawalls:

Seawalls are most often vertical walls protecting upland by preventing wave attack. They are emplaced at bluffs or other highlands with the beach or water on the opposite side. Well-designed seawalls, built on a rapidly eroding shoreline, will indeed protect the upland property. Seawalls do not, however, protect the beach in front and will move whatever erosion it is preventing on location to a downdrift coastal area.

Revetments:

Revetments are shore-parallel structures placed on a slope at the foot of bluffs, dunes, or along the beach face. This type of coastal protection device prevents landward erosion by creating wave breaking and loss of energy during the run-up process, limiting the reflection of wave energy from the beach. Revetments do not, however, protect the beach in front and will move whatever erosion it is preventing on location to a downdrift coastal area.

Groins:

Groins are barriers, usually, built perpendicular to the shoreline to impound the longshore transport of sediments. Groins provide local coastal protection against erosion, but the accretion of sediments on the updrift side of groins triggers a corresponding erosion, in the same order of magnitude, immediately downdrift of groins. This is evidently explained by the conservation of sand. Since the transport rate on a long straight beach is constant, the rate of sediment deposition against the groin must be equal to the rate of erosion. Hence, groins tend to transfer the problem of erosion further downcoast rather than yielding a sustainable solution to the problem.

Jetties:

Jetties are stone structures constructed at coastal inlets and navigational channels to prevent influx of sediments. Furthermore, jetties protect vessels from direct onslaught of waves. Similar to groins, jetties obstruct the longshore sediment transport causing substantial downdrift erosion.

Detached breakwaters:

Detached breakwaters are structures, typically, constructed seaward of the breaker line parallel to the shoreline. Detached (or offshore) breakwaters limit coastal erosion by reducing the amount of wave energy. Detached breakwaters does only in part, however, protect the beach in front and will move whatever erosion it is preventing on location to a downdrift coastal area.

Beach nourishment:

Long-term coastal erosion results from the fact that there is a sand deficit along the coastline. Beach nourishment (beach fill) is defined as artificial placement of beach material on an eroding segment of the shoreline to reduce the sand deficit. In this context, beach nourishment provides a protective measure that is in acceptable harmony with the natural circumstances as compared with hard coastal structures.

European experiences suggest that over the last decades soft coastal defense techniques are gradually gaining a greater acceptability as compared to classical hard coastal protection methods. Periodic artificial nourishment is widely regarded today as an environmentally-friendly method of beach and dune protection and restoration for short-term urgencies such as storm induced erosion, as well as long term issues, e.g. structural erosion and relative sea level rise (Hanson *et al.*, 2002).

6.2 No-action scenarios and proposed remedial measures

No-action scenario at the Power Plant

In the case where no measures are implemented to mitigate the problem at the beach by the power plant, the simulation period was just extended for 10 years after the verification simulation (see figure 6.1).

According to the simulation the accretion trend in the area will continue, and over 262,000 m^3 of sand is gained to the beach during the run. The sand transport rates generated by the model are continuously high but stable and the dredging problem will therefore continue to exist without diminishing in strength. However, in this case the model turns out to not be trustworthy in interpreting the shoreline exact position immediately to the west of the groin, where an unrealistic wedge occurs between the calculated shoreline and the groin. The wedge formation is caused by the large smoothing window parameter value (which specifies the number of cells that will be used in the calculations of the shoreline orientation affecting the wave transformation) and the abrupt change in shoreline position at the breakwater. However, calibration and verification simulations performed with lower smoothing window values resulted in less agreement between the final measured and calculated shorelines.

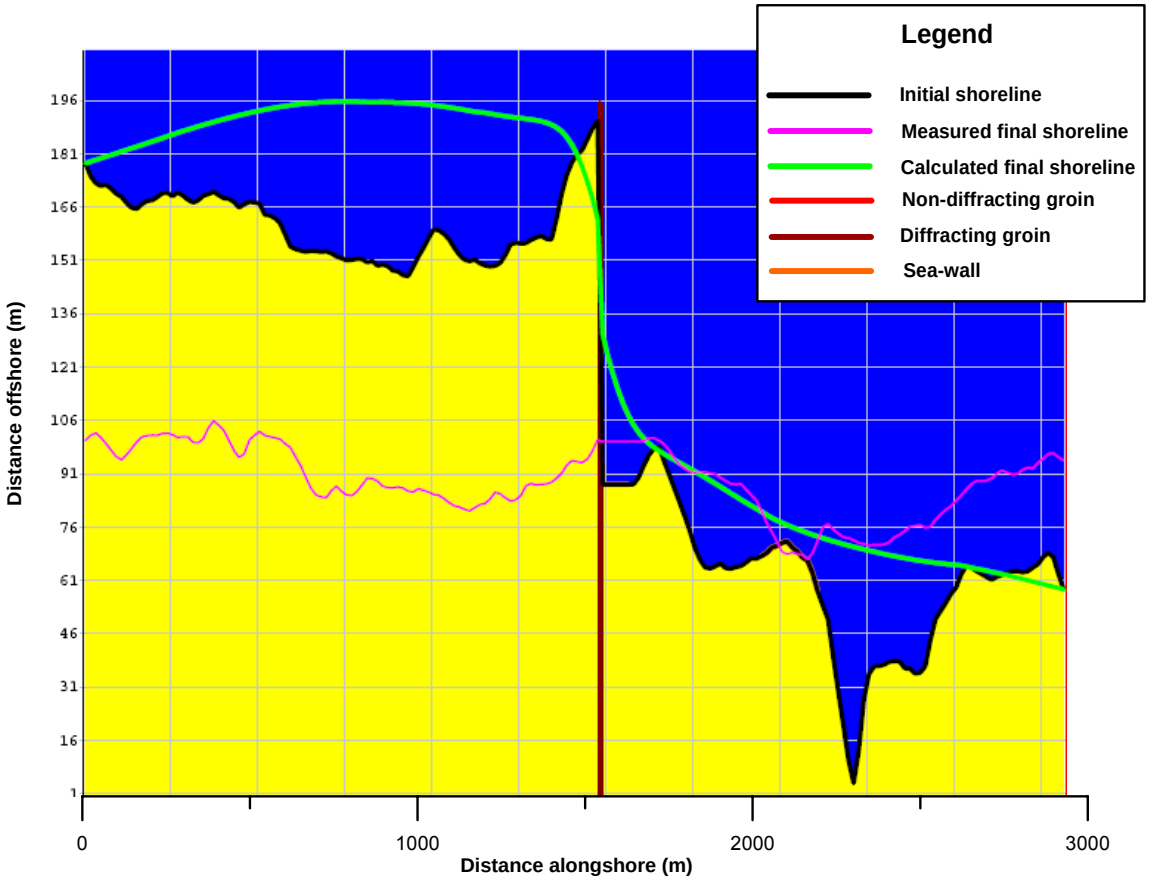

Figure 6.1 Result of a forecast simulation extending 10 years after the verification with no coastal measures implemented to the shoreline at the El Arish power plant.

Remedial measures at the El Arish Power Plant

Two remedial methods were investigated. The first one includes sand removal in the accretion area updrift the groin and sand nourishment downdrift of the groin. By increasing the breakwater length and introducing sand removal west of the breakwater, the bypassing at the breakwater has completely ceased (see figure 6.2). This measure will solve the dredging problem of the intake basin. Nevertheless, due to the large transport rates, great volume of sand has to be continuously removed updrift of the breakwater. During the simulation 319,000 m^3 of sand will have to be removed every year. The annual volume removed should, however, decrease after some years so that the retreat of the accretion area stops and the shoreline becomes stable. To stop the retreat of the shoreline, the removed volume of sand should not exceed the volume provided by the simulated westerly net transport rate of about 300,000 m^3. The simulation forecast starts in May, 1998 and runs for 10 years. By adjusting the location where the sand removal takes place, a mild change, instead of the excessive accretion-induced change, in the orientation of the new shoreline is achieved at the breakwater. As a result, the shoreline will be closer to an equilibrium state with the prevalent angle of incoming waves, and this measure will contribute to the reduction of the bypassing rate. In order to soften the shoreline and reduce the impacts from the currents caused by the discharger, the hard structure of the discharger is removed and replaced with a pipeline through which the effluent is discharged further seaward.

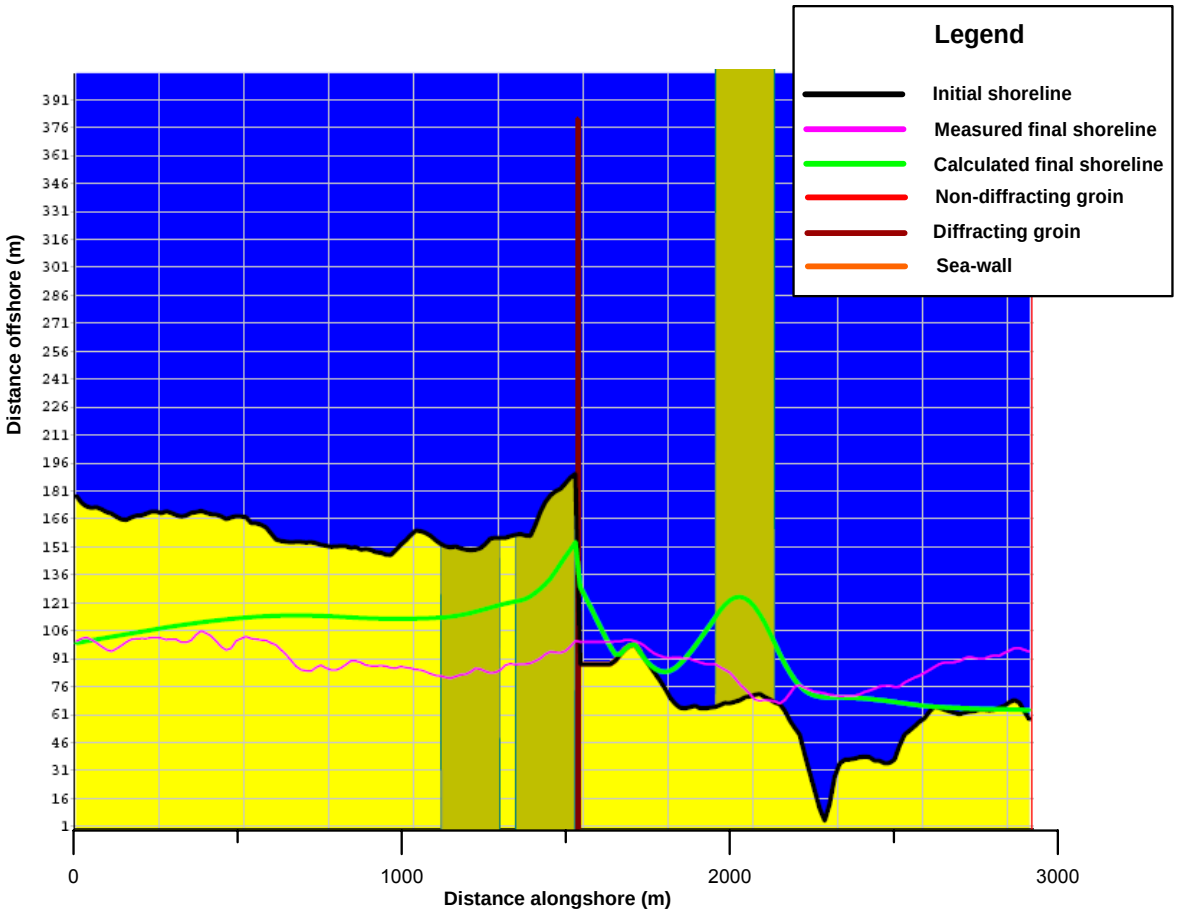

Figure 6.2 Result of a forecast simulation for El Arish power plant extending 10 years after verification simulation with sand removal updrift and sand nourishment downdrift of the intake basin implemented.

In the second alternative for remediation of the shoreline, the inlet and outlet of cooling water basin are replaced with pipelines under the seafloor. The inlet pipe will extend beyond the surf zone to prohibit sediments suspension in the intake water. The hard structures now present at the shoreline are removed from this spot. The shoreline will strive towards a new equilibrium state were no hard structure halts the nearshore transport, hence the beach stretch will return to a more natural state. However, the results of modeling this alternative did not depict the potential shoreline changes as, in fact, by removing all the hard structures no perturbation occurs in the shoreline, which is a prerequisite for shoreline modeling using GENESIS.

No-action scenario at the harbor

To examine the probable changes of the shoreline 10 years were added to the calibration simulation period and the model was run for a no-action scenario. As expected, the shoreline continues to accrete in the west and erode in the east (see figure 6.3). Immediately updrift of the breakwater the 2011 shoreline is likely to advance about 50 m as compared with 2001 shoreline. In the east of the harbor, at about 6100 m alongshore which is located between the harbor and the groin field the erosion causes the shoreline to retreat about 55 m. Also, the shoreline along the groin field starts to erode. At about 9200 m alongshore where most serious erosion occurs the shoreline retreats more than 80 m if no mitigation measure is applied. This trend will result in loss of the Palm Beach which is a beautiful beach resort at

the Sinai northern coast. For this reason, application of beach nourishment along this part of the beach is of utmost importance.

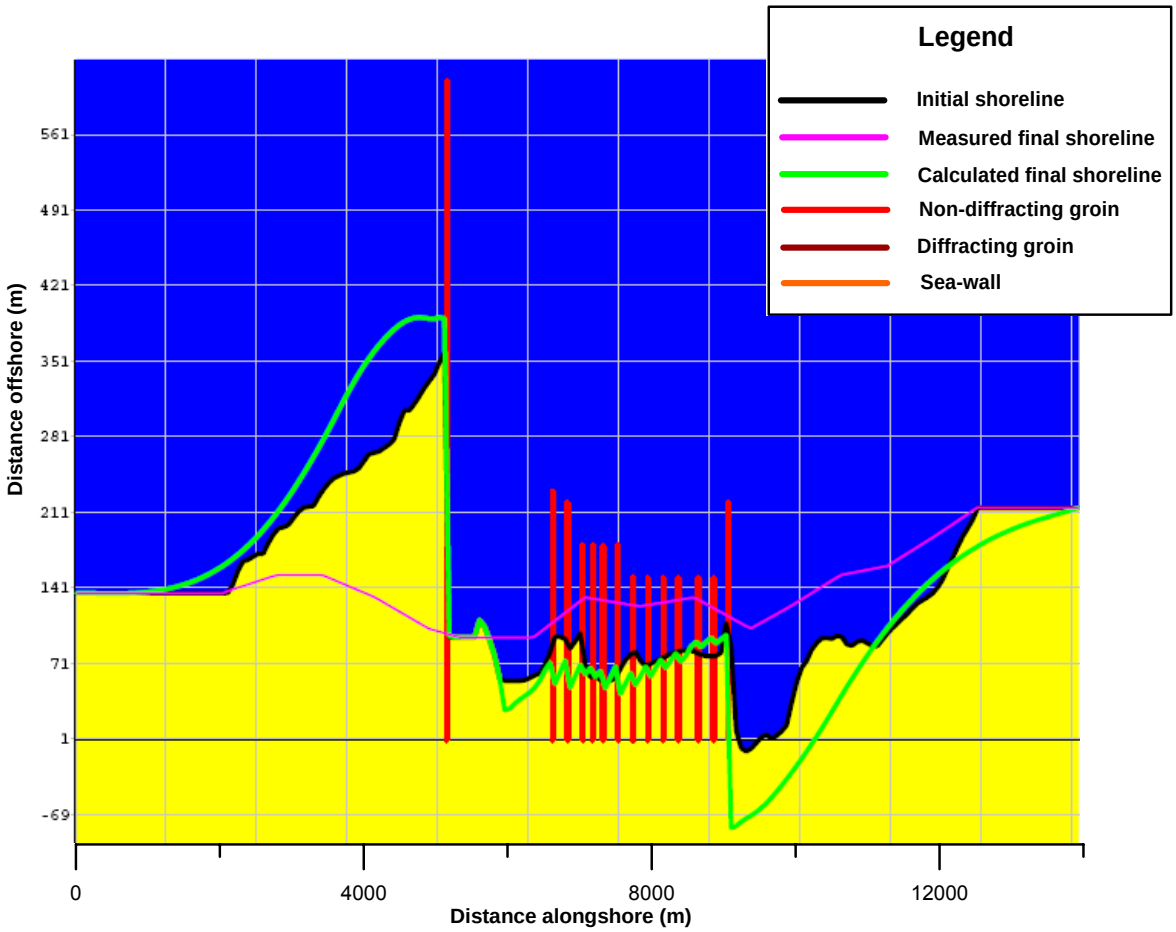

Figure 6.3 Shoreline change in no-action scenario for El Arish harbor.

Remedial measures at the El-Arish Harbor

Blockage of longshore sediment transport by the long breakwater of the harbor destabilized the downcoast beach in the form of erosion. Sediment entrapment by the groin field east of the harbor has resulted in local protection against erosion downdrift of the El-Arish harbor. Nevertheless, it is evident that this method has substantially altered the natural longshore movement of sediment. The model simulation period was extended with 10 years to see the effect of the nourishment scenario described below. The simulations started during 2001 and utilize the shoreline from the same year as the initial shoreline.

The calculated volume of the annual net transport rate is in the order of 110 000 m^3. This volume of littoral material is completely blocked at the harbor breakwater and no sediment can enter the harbor. GENESIS calculations reveal two erosion hotspots. These two eroding segments appear immediately downdrift of the harbor and groin field, where the latter is receding much more significantly. Therefore, considering the severe erosion downcoast of the groin field, it can be concluded that most of the sand is lost from this part of the beach.

The accretion part west of the breakwater is considered to be the borrow source for the littoral material. When simulating the nourished beach, a negative beach fill was applied to this segment, from the alongshore distance 4480 m to 5180 m, to represent the removal of material. A volume of 18,200 m^3 of this sand is then placed back on the beach from the alongshore distance 5950 m to 6650 m to maintain the shoreline between the harbor and the first groin. The remaining 92,800 m^3 should be transported to the part located between the alongshore distances of 9170 m and 9870 m to mitigate the erosion there (see figure 6.4). The sediment provided, from the borrow source can be transported mechanically to the nourishment site immediately downdrift of the groin field using land-based methods. Another method to bypass sediments is the installation of a pipeline together with supplemental pumping station. Net sediment transport rates were checked for each individual year of the simulation period to ensure that no by passing was taking place at the breakwater.

Creation of a feeder beach downdrift of the groin field is recommended. The unidirectional eastward sediment transport along the Sinai northern coast distributes the fill material farther downcoast. According to CEM (part 5, 2002), feeder beaches can be applied in areas that are presently suffering deficit in the supply of littoral material and have unusually high loss rates, and also, in areas where the net longshore transport rate is predictable and the net longshore transport in one direction greatly exceeds the net longshore sediment transport in the other direction.

Beach nourishment is intended to widen the eroding beach and form an erosional buffer zone. Coastal erosion is an ongoing process and the nourished sand erodes away after sufficient amount of time has elapsed. The beach shall be renourished periodically such that the erosional buffer zone is rebuilt. In addition to protecting the shoreline from erosion, beach nourishment has recreational advantages as well and, therefore, best suits touristic beach resorts.

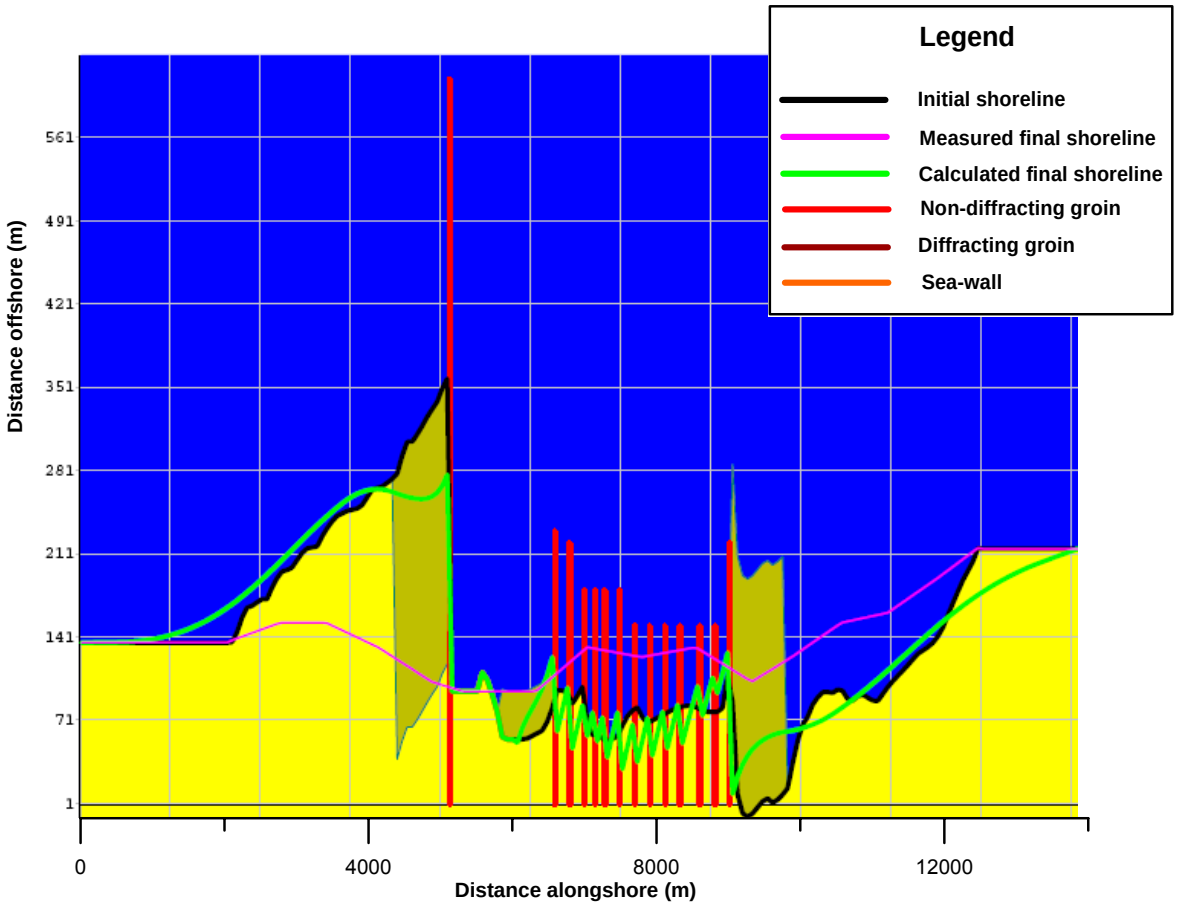

Figure 6.4 The simulated effect of sand removal west of the breakwater together with beach nourishment at the downdrift of the groin field (beach nourishment prevents further erosion in 2011 as compared with no action scenario).

Conclusion

The northern coast of the Sinai Peninsula has been subjected to appreciable changes that are intensified by human influence on the coastline. Placement of coastal infrastructures at El Arish has obstructed the longshore sediment transport which has resulted in shoreline advance/retreat. Wave-induced longshore currents were found to be responsible for transporting the littoral drift along the coastline. Appropriate protective measures should be set in place to control the destructive impacts of coastal erosion as well as minimize the maintenance costs of the infrastructure in a sustainable way.

Mathematical modeling of the longshore sediment transport revealed that the predominant direction of transport is towards east which is also indicated by the accretion-erosion trend of shoreline change on either sides of coastal structures. Furthermore, gradients in the sediment transport highlight the approximate location of accretion-erosion areas along the coast. According to the mathematical modeling, the El Arish shoreline is located in an accretion area where the littoral drift converges. The calculated volumes of sediment transport rate using the CERC formula is, however, not site specific as no previous estimation of sediment transport rate was available to calibrate the mathematical model.

The area west of El Arish Power Plant has accreted to the full capacity and the littoral drift is bypassing the tip of the breakwater of the cooling water intake basin. Results of the shoreline change modeling of the power plant show that, for example, in 1998 the littoral drift bypassed the breakwater at a rate of 271,000 m^3/year. This volume of sediment is entrapped in the cooling water intake basin/channel and must be removed artificially in order for the basin to remain functional.

Using the shoreline change model GENESIS two remediation scenarios were modeled to alleviate the sedimentation problem at El Arish Power Plant. The first scenario comprises sand removal in the accretion area updrift the western breakwater of the power plant. The discharger is suggested to be replaced with a pipeline to eliminate the obstructive impact of the hard structure and the effluent on the sediment transport. The breakwater length is increased and sand supplied from the west of the breakwater is mechanically placed back on the beach east of the intake channel. Implementation of a pumping station to transport the sediments from the accretion area to the beach downcoast of the breakwater would be a suitable alternative method as the volume of sand to be bypassed is ample. In the second alternative, all hard coastal structures of the cooling water intake basin and discharger are proposed to be removed and replaced with two pipelines. The pipeline for cooling water shall be extended beyond the depth of closure so as to avoid damage caused by sediment load in the cooling water. Similarly, disturbances to the longshore sediment transport can be eliminated if the discharger pipeline is extended beyond the closure depth.

At El Arish Harbor the predominant longshore sediment transport is completely blocked by the western breakwater and no sediment can bypass the harbor. A large area of accretion west of the breakwater clearly indicates this trend. The expanding area of accretion is not a major concern as yet, since the harbor's western breakwater is too long for the sediment to bypass and cause sedimentation inside the harbor. However, this obstruction has brought about a sand deficit east of the harbor triggering ongoing severe erosion. Although, construction of the groin field in this area has provided local shoreline protection, it has also

transferred the erosion eastward to the palm beach. The sediment deficit must be compensated for artificially to prevent further erosion without transferring the problem downcoast.

Sand-bypassing/beach-nourishment is proposed to mitigate the erosion problem east of the groin field. The nourishment material can be provided from the accretion area west of the Harbor. Based on the GENESIS simulation, to prevent further accretion, annually 110,000 m^3/year shall be taken up from the borrow site. Placement of this material on the immediate downdrift of the groin field will help alleviate the severe erosion at the palm beach. This volume of material will be bypassed mechanically using land-based methods. Installation of a pipeline together with pumping station could be another method for transporting the sediments to the nourishment site.

Application of soft methods of coastal protection, e.g. beach nourishment, can help mitigate coastal erosion problems with minimal side effects. Instead of striving to fully control the forces of nature, for example by using hard engineering structures, coastal protection must be provided in a way that works in harmony with the nature of coastal areas. Accretion areas create best borrow sources for nourishment materials at the Sinai northern coast. Abundance of sand sources also suggests that nourishment material can be conveniently provided to the eroding areas. Therefore, in this study, execution of beach nourishment to remedy erosion problem is preferred over hard solutions.

Literature Cited

Abdel Rahman, S.I., M.H. Ahmed. and Essa, M.M., 2001, "Drought Monitoring in the Southeastern Mediteranean Basin using Satellite Data" Proceedings of The International Geographic and Remote Sensing Symposium, IGARSS 2001,July 19-23, Sydney, Australia.,

Badr, A.M., 2001,"Modeling, Measurments and Control", Association for the Advancement of Modeling and Simulation Techniques in Enterprises 2001-vol. 62.

CEM, 2002, "Coastal Engineering Manual", Coastal and Hydraulics Laboratory (CHL), Engineer Research and Development Center (ERDC), Vicksburg, Mississippi.

Dean, R.G. and Dalrymple, R.A., "Coastal Processes with Engineering Applications", 2002, University of Florida and University of Delaware, Cambridge University Press.

Dahlerus, C.J. and Egermayer, D., 2005 "Uppspolning och klittererosion längs Ystadkusten - Situation idag och framtida scenarier", Master thesis, Lund University, Sweden.

Danish Hydraulic Institute (DHI), n.d., "Report on Suez Channel", Appendix A, Offshore wave and wind conditions.

Delft Hydraulics, 1999, "Port Said East Port, Egypt", unpublished report.

Dewidar, KH. M. and Frihy O. E., 2003, "Thematic Mapper Analysis to Identify Geomorphologic and Sediment Texture of El Tineh Plain, North-western Coast of Sinai, Egypt", INT.J. Remote Sensing, Vol.24, No.11, 2377-2385.

Fanos, A.M., Khafayg, A.A., Anwar, M.N., Naffaa, M.G.,n.d., 1994, "Assessment and Recommendations for the Enhancement of the Bardawil Lagoon Outlets", Coastal Research Institute, Alexandria, Egypt.

Fenoglio-Marc, L. 2001, "Long-term Sea Level Change in the Mediterranean Sea from Multi-satellite Altimetry and Tide Gauges", Physics and Chemistry of the Earth, In proceedings of EGS general assembly, Nice.

Frihy, O.E., Badr, A.A., Selim, M.A., El Sayed, W.R., 2002. "Environmental Impacts of El Arish Power Plant on the Mediterranean Coast of Sinai, Egypt", Environmental Geology, 42:604-611.

Frihy, O.E., and Lofty, M.F., 1997. "Shorline Change and Beach-sand Sorting Along the Northern Sinai Coast of Egypt", Geo-Marine Letters, 17:140-146.

Hamed, Y., 2007, unpublished report.

Hanson, H., Brampton, A., Capobianco, M., Dette, H.H., Hamm, L., Laustrup, C., Lechuga, A., Spanhoff, R., 2002, "Beach Nourishment Projects, Practices, and Objectives-a European Overview", Coastal Engineering 47(2002) 81-111.

Hanson, H. and Kraus, N.C., 1989 "GENESIS: Generalized Model for Shoreline Change, Report1, Technical Reference", Technical Report CERC-89-19, US Army Corps of Engineers.

Hellström, B., 1953, "The Ground Water Supply of North-Eastern Sinai", Geografiska Annaler, Vol. 35, No. 2. (1953), 61-74

Inman, D.L., 2003, "littoral cells", Kluwer Academic Publishers, Dordrecht, The Netherlands.

Komar, P.D , 1976, "Beach Processes and Sedimentation", Prentice-Hall, INC., Englewood Cliffs, NJ

Millot, C. and Toupier-Letage, I., 2004, "Circualtion in the Mediterranean Sea", The Handbook in Environmental Chemistry, Vol. 1, Springer-Verlag Editor.

Larsen, G.C. and Hansen K.S., 2001, "Database on Wind characteristics, Users Manual", Risø National Laboratory, Roskilde, Denmark.

Larson, M. and Hanson, H., 1992. "Analys av Klimatologiska och Hydrografiska Data för Ystadsbukten", Report 3159, Water Resources, Lund University Faculty of Engineering, Lund, Sweden.

Larson, M., Kraus, N. C. and Hanson, H., 2002. "Simulation of regional longshore sediment transport and coastal evolution – the "Cascade" model", Proceedings 28th Coastal Engineering Conference, World Scientific Press.

Pethick, J.S., 1984, "An introduction to coastal geomorphology", Edward Arnold Publishers, Baltimore, MD

Pinardi, N. and Masetti, E., 2000, "Variability of the large scale general circulation of the Mediterranean Sea from observations and modelling: a review", Palaeogeography, Palaeoclimatology, Palaeoecology 158 (2000) 153–173.

Robaa, S.M., 2002, "Urban-suburban/rural Differences over Greater Cairo, Egypt" Atmósfera(2003), 157-171.

Rosen, D.S., 2002, "Long Term Remedial Measures of Sedimentological Impact due to Coastal Development on the South Eastern Mediterranean Coast", Littoral 2002, The Changing Coast, 321-331.

SPM, 1984, "Shore Protection Manual", Department of the Army, Coastal Engineering Research Center, Vicksburg, Mississippi.

Stanley, D.J., Nir, Y. and Galili, E.,1997. "Clay Mineral Distribution to Interpret Nile Cell Provenance and Dispersal: III. Offshore Margin between Nile Delta and Northern Israel", Journal of Coastal Research, 14(1), 196-217, Royal Palm Beach.

"Wind Atlas of Egypt", 2005, New and Renewable Energy Authority, Egyptian Meteorological Authority and Risø National Laboratory.